A time-varying parameter estimation approach using split-sample calibration based on dynamic programming

Xiaojing Zhang[a,b], Pan Liu[a,b*]

[a]State Key Laboratory of Water Resources and Hydropower Engineering Science, Wuhan University, Wuhan 430072, China

[b]Hubei Provincial Key Lab of Water System Science for Sponge City Construction, Wuhan University

*Corresponding author. Email: liupan@whu.edu.cn;

Tel: +86-27-68775788; Fax: +86-27-68773568

Abstract: Although the parameters of hydrological models are usually regarded as constant, temporal variations can occur in a changing environment. Thus, effectively estimating time-varying parameters becomes a significant challenge. Two methods, including split-sample calibration (SSC) and Data assimilation, have been used to estimate time-varying parameters. However, SSC is unable to consider the parameter temporal continuity, while Data assimilation assumes parameters vary at every time-step. This study proposed a new method that combines (1) the basic concept of split-sample calibration (SSC), whereby parameters are assumed to be stable for one sub-period, and (2) the parameter continuity assumption, i.e., the differences between parameters in consecutive time steps are small. Dynamic programming is then used to determine the optimal parameter trajectory by considering two objective functions: maximization of simulation accuracy and maximization of parameter continuity. The efficiency of the proposed method is evaluated by two synthetic experiments, one with a simple two-parameter monthly model and the second using a more complex 15-parameter daily model. The results show that the proposed method is superior to SSC alone, and outperforms the ensemble Kalman filter if the proper sub-period length is used. An application to the Wuding River basin indicates that the soil water capacity parameter varies before and after 1972, which can be interpreted according to land use and land cover changes. A further application to the Xun River basin shows that parameters are generally stationary on an annual scale, but exhibit significant changes over seasonal scales. These results demonstrate that the proposed method is an effective tool for identifying time-varying parameters in a changing environment.

Keywords: hydrological model; time-varying parameter; calibration; dynamic programming

1. Introduction

Conceptual models describe the physical processes that occur in the real world by means of certain assumptions and empirically determined functions (Toth and Brath, 2007). In spite of their simplicity, conceptual models are effective in providing reliable runoff predictions for widespread applications (Quoc Quan et al., 2018; Refsgaard and Knudsen, 1996), such as real-time flood forecasting, climate change impact assessments (Deng et al., 2019; Stephens et al., 2019), and water resources management. Conceptual hydrological models typically have several inputs, a moderate number of parameters, state variables, and outputs. Among these, the parameters play an important role in accurate simulation and should be related to the catchment properties. However, parameter values often cannot be obtained by field measurements (Merz et al., 2011). An alternative approach is to calibrate parameters based on historical data.

Parameters are usually regarded as constants in time scale, because of the general idea that catchment conditions are temporally stable. Constant parameters become inaccurate in differential split-sample test (DSST) conditions (Klemes, 1986). For example, parameters calibrated based on data from a wet (or dry) period may fail to simulate runoff in a dry (or wet) period for the same catchment. Broderick et al. (2016) used DSST to assess the transferability of six conceptual models under contrasting climate conditions. They found that performance declines most when models are calibrated during wet periods but validated in dry ones. Fowler et al. (2016) pointed out that the parameter set obtained by mathematical optimization based on wet periods may not be robust when applied in dry periods. Additionally, the catchment properties can

change over time, such as in the case of afforestation and deforestation (Guzha et al., 2018; Siriwardena et al., 2006). These changes need to be taken into account through model parameters (Bronstert, 2004; Hundecha and Bardossy, 2004). Hence, temporal variations in parameters should reflect the changing environment.

One challenge here is the methodology used to identify time-varying parameters. In the literature, three approaches have been discussed. The first is split-sample calibration (SSC), whereby available data are split into a moderate number of sub-periods and the parameters are calibrated individually for each period (Thirel et al., 2015). The second method is data assimilation (Deng et al., 2016; Pathiraja et al., 2018). This method assimilates observational data to enable errors, states, and parameters to be updated (Li et al., 2013), making it possible to identify time-varying parameters. The third approach is to construct a functional form or empirical equation according to the correlation between parameters and some climatic variates such as precipitation and potential evapotranspiration (Deng et al., 2019; Jeremiah et al., 2013; Westra et al., 2014). Note that this study focuses on methods to identify time-varying parameters rather than modelling them; hence, only comparisons between SSC and data assimilation are discussed.

SSC is the most commonly used method (Coron et al., 2012; Fowler et al., 2018; Paik et al., 2005; Xie et al., 2018). Merz et al. (2011) investigated the time stability of parameters by estimating six parameter sets based on six consecutive five-year periods. Lan et al. (2018) clustered calibration data into 24 sub-annual periods to detect the seasonal hydrological dynamic behavior. Despite broad application, it remains

69 debatable whether a particular mathematical optimum gives the parameter value during
70 one period. Many equivalent optima can exist simultaneously for one dataset when
71 calibrating the model against observations (Poulin et al., 2011). Several studies
72 addressed this question by adding more constraints to the objective function over the
73 respective period. For example, Gharari et al. (2013) emphasized consistent
74 performance in different climatic conditions, while Xie et al. (2018) modified SSC by
75 selecting parameters with good simulation ability for both the current sub-period and
76 the whole period. Some conceptual hydrological parameters reflect the catchment
77 characteristics. While climate change and human activities exert influence on these
78 catchment characteristics, they can hardly change dramatically in a very quick time,
79 such as the soil water storage capacity. Hence, parameter continuity, defined as
80 differences between the parameters in consecutive time steps to be small, is required
81 for hydrological modeling. However, few reports have considered the continuity of
82 parameters in the SSC method.

83 This assumption of parameter continuity is the basic idea behind data assimilation
84 methods. For example, the a priori parameters in ensemble Kalman filter (EnKF)
85 methods are commonly derived from updated values from the previous time step
86 (Moradkhani et al., 2005; Xiong et al., 2019). From this, a trade-off between simulation
87 accuracy and parameter continuity is established, and parameters that enable greater
88 continuity are more likely to be selected. Deng et al. (2016) validated the ability of the
89 EnKF to identify changes in two-parameter monthly water balance (TMWB) model
90 parameters. Pathiraja et al. (2016) proposed two-parameter evolution models for

improving conventional dual EnKF and obtained superior results for diagnosing the non-stationarity in a system. EnKF and its variants are relatively advanced approaches for identifying time-varying parameters (Lu et al., 2013). However, for a hydrological model, the states may change over every time step, whereas the parameters may not, in particular for hourly time scales. This can be offset by SSC, which assumes that the parameters remain stable for a pre-determined period (such as decades, years, or months). Compared to EnKF, the simplicity of SSC is another advantage, as it has a less complex mechanism and reduced redundancy (Chen and Zhang, 2006).

The aim of this study is to present a new method for time-varying parameter estimation by combining the strengths of the basic concept of SSC and the continuity assumption of data assimilation, which is a useful tool for diagnosing the non-stationarity caused by a changing environment. Compared with data assimilation, the proposed split-sample calibration based on dynamic programming (SSC-DP) avoids overly frequent changes of parameters, such as hourly or daily variations. Compared with SSC, the distinctive element is that SSC-DP considers the parameters to be related over adjacent sub-periods, and selects parameter sets with good performance for each period and small differences between adjacent time steps. In this study, three aspects of the proposed method are evaluated: (1) The performance of SSC-DP is compared with that of existing methods in terms of the estimation of time-varying parameters; (2) The applicability of SSC-DP to more complex hydrological models with a considerable number of parameters; (3) The ability of SSC-DP to provide additional insights on parameter variations and their correlations with the properties of real catchments. To

investigate the above issues, the proposed method is compared with SSC and EnKF in two synthetic experiments (one with a two-parameter monthly model, the other with a 15-parameter daily model). SSC-DP is also applied to two real catchments for parameter estimation under different environmental conditions.

The remainder of this paper is organized as follows. Section 2 describes the proposed method, reference methods, and performance evaluation indices. Section 3 describes two synthetic experiments and two real catchment case studies for comparison among different time-varying parameter estimation methods. Sections 4 and 5 present the results and discussion, respectively, before the conclusions to this study are drawn in Sect. 6.

2. Methodology

In this section, a SSC-DP method is proposed to identify the time-varying parameters of hydrological models. The two hydrological models considered in this study are the TMWB and Xinanjiang models. Their concepts and differences are presented in Sect. 2.1. A sensitivity analysis is employed to focus efforts on parameters important to calibration and avoid prohibitive computational cost, as outlined in Sect. 2.2. Three time-varying parameter estimation methods (SSC, SSC-DP, and data assimilation) are presented in Sect. 2.3. The SSC and data assimilation are provided for comparisons with the SSC-DP. Finally, to evaluate the performance of the time-varying parameter estimation methods, six evaluation criteria are selected and formulated in Sect. 2.4. The flowchart of the methodologies is shown in Fig. 1.

2.1 Hydrological models

2.1.1 Two-parameter monthly water balance model

The TMWB model developed by Xiong and Guo (1999) is efficient for monthly runoff simulations and forecasts (Dai et al., 2018; Guo et al., 2002; Kim et al., 2016; Yang et al., 2017). The model requires monthly precipitation and potential evapotranspiration as inputs. Its simplicity and efficiency of performance mean that TMWB can easily be used to investigate the impacts of climate change (Deng et al., 2016; Luo et al., 2019). Its outputs include monthly streamflow, actual evapotranspiration, and soil moisture content index. The model has only two parameters (Table 1), *C* and *SC*. The parameter *C* takes account of the effect of the change of time scale when simulating actual evapotranspiration. The parameter *SC* represents the field capacity (mm).

2.1.2 Xinanjiang model

The Xinanjiang model (Zhao, 1992) is widely used in China (Li and Zhang, 2017; Si et al., 2015; Yin et al., 2018). It takes precipitation and pan-evaporation data as inputs and estimates the actual evapotranspiration, soil moisture storage, surface runoff, interflow, and groundwater runoff from the watershed. The simulated streamflow is calculated by summing the routing results of the surface, interflow, and groundwater runoff (Sun et al., 2018). In this study, the surface runoff is routed by the instantaneous unit hydrograph (Lin et al., 2014), while the interflow and groundwater runoff are routed by the linear reservoir method (Jayawardena and Zhou, 2000). A schematic

155 overview of the model is presented in Fig. 2. The meaning, range and units of all the
156 parameters in the Xinanjiang model are listed in Table 2.

157 There are two important differences between the TMWB and Xinanjiang models:
158 (1) the TMWB model has two parameters, while the Xinanjiang model has fifteen
159 parameters; (2) TMWB is a monthly rainfall-runoff model, whereas the Xinanjiang
160 model can run on hourly or daily step sizes.

161 **2.2 Parameter sensitivity analysis method**

162 Sensitivity analysis is used to identify which parameters significantly affect the
163 performance of the Xinanjiang model and reduce the number of parameters to be
164 calibrated. Numerous sensitivity analysis methods are available, such as the Morris
165 method (Morris, 1991) and Sobol analysis (Sobol, 1993). The Morris method provides
166 similar results to Sobol analysis with a reduced computational burden (Rebolho et al.,
167 2018; Teweldebrhan et al., 2018; Yang et al., 2018).

168 The Morris method assumes that if parameters change by the same relative amount,
169 the parameter that causes the larger elementary effect is the more sensitive (King and
170 Perera, 2013). The elementary effect is calculated as follows:

171 $$EE_p(\theta_1,\theta_2,...,\theta_{Np},\Delta)=\frac{y(\theta_1,\theta_2,...,\theta_{p-1},\theta_p+\Delta,\theta_{p+1},...,\theta_{Np})-y(\theta_1,\theta_2,...,\theta_{Np})}{\Delta} \quad (1)$$

172 where θ_p represents the p-th parameter; Δ is the relative amount; Np is the total
173 number of parameters, and y is the model output based on a particular parameter set.

174 Each parameter is changed in turn and every parameter set produces an elementary
175 effect. The parameter sensitivity is evaluated using the mean value μ of the

elementary effects. If a parameter has a higher value of μ, it is more sensitive. In fact, interactions between parameters should be taken into account (Jie et al., 2018). Hence, the standard deviation σ can be calculated. A higher value of σ indicates a stronger nonlinear correlation between parameters (Pappenberger et al., 2008).

2.3 Time-varying parameter estimation method

2.3.1 Split-sample calibration

SSC provides a simple way of diagnosing parameter non-stationarity under a changing environment (Merz et al., 2011). As illustrated in Fig. 3(a), the method usually has two steps (Hughes, 2015; Kim et al., 2015): (1) Available data are divided into several consecutive periods, which can be arbitrarily chosen as hours, days, months, seasons, or years; (2) Parameters are calibrated separately for the respective period. This procedure gives better simulation performance than using constant parameters, but leads to the estimated parameters fluctuating strongly over adjacent sub-periods, producing false temporal variants.

2.3.2 Split-sample calibration based on dynamic programming

To overcome this problem, the SSC-DP method identifies time-varying parameters with consideration of temporal continuity. SSC-DP has five steps (Fig. 3(b)):

(1) Split-sample periods. This process is the same as the first step of the SSC.

(2) Generate an ensemble of near-optimal parameters. Multiple parameter sets having objective values close to the optimum for each sub-period are obtained using Markov chain Monte Carlo (MCMC) sampling (Chib and Greenberg, 1995). The

likelihood measure of the *i*-th sub-period links the parameter to observations using the Nash–Sutcliffe efficiency (NSE) (Nash and Sutcliffe, 1970) as follows:

$$L_i(\theta) = 1 - \frac{\sum_{t=(i-1)\times l+1}^{i\times l} (Q_t - \widehat{Q}_t)^2}{\sum_{t=(i-1)\times l+1}^{i\times l} (Q_t - \overline{Q_t})^2} \tag{2}$$

where Q_t and $\widehat{Q}_t$ are the observed and simulated runoff at time step t, respectively, and l is the length of the sub-period.

(3) Optimize by using Dynamic programming. The goal is to find parameters that provide both accurate streamflow simulations and continuity. The continuity condition aims to minimize the difference between the estimated parameters for sub-periods *i* and *i*+1. For *N* sub-periods, the objective function can be expressed as follows:

$$\text{Max } F = \sum_{i=1}^{N}[(\text{NSE}_i + \text{NSE}_{ln,i} + \text{NSE}_{abs,i}) - \alpha \times \sum_{p=1}^{N_P} \frac{|\theta_{i+1,p} - \theta_{i,p}|}{\theta_{max,p} - \theta_{min,p}}] \tag{3}$$

$$NSE_{\ln,i} = 1 - \frac{\sum_{t=(i-1)\times l+1}^{i\times l} (\ln(Q_t) - \ln(\widehat{Q}_t))^2}{\sum_{t=(i-1)\times l+1}^{i\times l} (\ln(Q_t) - \ln(\overline{Q_t}))^2} \tag{4}$$

$$NSE_{abs,i} = 1 - \frac{\sum_{t=(i-1)\times l+1}^{i\times l} \left|Q_t - \widehat{Q}_t\right|}{\sum_{t=(i-1)\times l+1}^{i\times l} \left|Q_t - \overline{Q_t}\right|} \tag{5}$$

where $\theta_{i,p}$ is the *p*-th estimated parameter over the *i*-th sub-period; $\theta_{max,p}$ and $\theta_{min,p}$ are its maximum and minimum values, respectively; N_P is the number of the parameters; and α is the weight, reflecting parameter continuity. The weights of NSE_i, $\text{NSE}_{ln,i}$, and $\text{NSE}_{abs,i}$ are set to 1 following the work of Merz et al. (2011), who used equal weights for the NSE and its variants.

As the decision-making process during the current sub-period is related to that of the previous sub-period, the parameter estimation over N periods becomes a multi-stage optimization problem. To solve this, a dynamic programming technique (Bellman, 1957) is employed to decompose the optimization into a number of single-stage problems and determine the optimal trajectory of the time-varying parameters. Dynamic programming is a useful method for handling sequential operation decisions. It allows the problem to be solved using a backward recursive procedure, whereby the decision-making for each sub-period maximizes the sum of current and future benefits (Li et al., 2018; Ming et al., 2017). In this study, the objective function is formulated as the following recursive equation:

$$\begin{cases} F_i^* = max\{f_i[\vartheta_{i,1}, \vartheta_{i,2}, \vartheta_{i,3}, \cdots, \vartheta_{i,p}] + F_{i+1}^*\} \\ F_N^* = 0 \end{cases} \quad (6)$$

where F_i^* is the evaluation index using the optimal time-varying parameters from the N-th to the i-th sub-periods, and Eq. (6) calculates the objective function from the N-th sub-period to the first sub-period.

(4) Update initial states. The initial states, such as that of the soil water content, are important in model simulation and calibration. As the final states for sub-period i are not used as the initial states for sub-period i+1 during steps (1)–(3), the time-varying parameter set obtained from step (3) is applied to the hydrological model to update the initial states of each sub-period for the next iteration.

(5) Steps (1)–(4) are repeated until the initial states of each sub-period are generally stable.

2.3.3 Data assimilation

Another approach for diagnosing variations in parameters is data assimilation, using methods such as the EnKF and ensemble Kalman smoother (EnKS). These are used here as reference methods. The EnKF has been widely applied to conceptual models, including TMWB (Deng et al., 2016). Li et al. (2013) noted that the EnKF struggles to handle the time-lag in routing processes. However, the routing component is vital to the Xinanjiang model. EnKS can efficiently determine the states of the Xinanjiang model (Meng et al., 2017), but the estimation of routing parameters deserves discussion. Most previous studies have used a fixed distribution of the routing hydrograph in data assimilation (Lu et al., 2013), i.e., the parameters are constant for routing processes. With respect to these issues, a modified EnKF (named SSC-EnKF) is established as a third data assimilation reference method in the synthetic experiment with the Xinanjiang model (described in Sect. 3.1).

The EnKF includes two main steps: model prediction and assimilation. The state vector is augmented with parameter variables so that time-varying parameters can be estimated simultaneously with model states. For model prediction, the augmented vector is derived by adding noise on that from the previous time step through the following equation:

$$\begin{pmatrix} \vartheta_{t+1}^{k-} \\ x_{t+1}^{k-} \end{pmatrix} = \begin{pmatrix} \vartheta_{t}^{k+} \\ f\left(x_t^{k+}, \theta_{t+1}^{k-}, u_{t+1}\right) \end{pmatrix} + \begin{pmatrix} \delta_t^k \\ \varepsilon_t^k \end{pmatrix},\ \delta_t^k \sim N\left(0, R_t\right), \varepsilon_t^k \sim N\left(0, G_t\right) \tag{7}$$

where ϑ_t is the parameter vector at time step t, represented as $\left(\theta_{t,1}, \theta_{t,2}, ..., \theta_{t,Np}\right)$; x_t is the state vector; ϑ_{t+1}^{k-} and x_{t+1}^{k-} are the *k*-th ensemble member forecasts at time step

t+1; ϑ_t^{k+} and x_t^{k+} are the updated values of the k-th ensemble member forecasts at time step t; u_{t+1} denotes the forcing data (e.g., precipitation) at time step t+1; δ_t^k and ε_t^k are the white noise for the k-th ensemble member, which follow a Gaussian distribution with zero mean and specified covariance of R_t and G_t, respectively.

In the assimilation process, the augmented vector is updated using the following equations if suitable observations are available:

$$\begin{pmatrix} x_{t+1}^{k+} \\ \vartheta_{t+1}^{k+} \end{pmatrix} = \begin{pmatrix} x_{t+1}^{k-} \\ \vartheta_{t+1}^{k-} \end{pmatrix} + \begin{pmatrix} K_{t+1}^{x} \left[y_{t+1}^{k} - \hat{y}_{t+1}^{k} \right] \\ K_{t+1}^{\vartheta} \left[y_{t+1}^{k} - \hat{y}_{t+1}^{k} \right] \end{pmatrix} \tag{8}$$

$$y_{t+1}^{k} = y_{t+1} + \xi_{t+1}^{k},\ \xi_{t+1}^{k} \sim N(0, W_t), \tag{9}$$

$$\hat{y}_{t+1}^{k} = h(x_{t+1}^{k-}, \vartheta_{t+1}^{k-}) \tag{10}$$

where y_{t+1} is the observation vector at time t+1; y_{t+1}^k is the k-th observation ensemble member at time step t+1; $\hat{y}_{t+1}$ is the simulation vector at time t+1; h is the observational operator that converts the model states to observations; ξ_{t+1}^k is the measurement error, which follows a Gaussian distribution with a covariance of W_t; and K_{t+1}^k is the Kalman gain matrix (for details, see (Feng et al., 2017).

The EnKS is based on the EnKF. Whereas the EnKF updates the model states and parameters at the current time step, the EnKS takes account of those values over the past time steps. The main steps of the EnKS are identical to those of the EnKF, but the equation of the assimilation process is formulated as follows:

$$\begin{pmatrix} x_{t+1\to t-n+2}^{k+} \\ \vartheta_{t+1\to t-n+2}^{k+} \end{pmatrix} = \begin{pmatrix} x_{t+1\to t-n+2}^{k-} \\ \vartheta_{t+1\to t-n+2}^{k-} \end{pmatrix} + \begin{pmatrix} K_{t+1}^{x*} \left[y_{t+1}^{k} - \hat{y}_{t+1}^{k} \right] \\ K_{t+1}^{\vartheta*} \left[y_{t+1}^{k} - \hat{y}_{t+1}^{k} \right] \end{pmatrix} \tag{11}$$

$$\hat{y}_{t+1}^{k} = h(x_{t+1\to t-n+2}^{k-}, \vartheta_{t+1\to t-n+2}^{k-}) \tag{12}$$

where K_{t+1}^{*} is the Kalman gain matrix of EnKS. The fixed time window n of EnKS

277 is pre-determined based on the response function or unit hydrograph. Meng et al.
278 (2017) suggested that the time window should be set as half of the recession time of
279 a flood.

280 A third data assimilation approach is constructed based on the SSC. Instead of
281 assimilating one observed variable, it assimilates the observed variables during a given
282 period in one assimilation process. Assuming that the parameters are constant in the
283 given period, the equation of the assimilation process for the *i*-th sub-period is
284 expressed as follows:

285 $$\begin{pmatrix} x_{i+1}^{k+} \\ \vartheta_{i+1}^{k+} \end{pmatrix} = \begin{pmatrix} x_{i+1}^{k-} \\ \vartheta_{i+1}^{k-} \end{pmatrix} + \begin{pmatrix} K_{i+1}^{x^*} \left[y_{i\times l+1\to(i+1)\times l,}^{k} - \widehat{y}_{i\times l+1\to(i+1)\times l}^{k} \right] \\ K_{i+1}^{\vartheta^*} \left[y_{i\times l+1\to(i+1)\times l}^{k} - \widehat{y}_{i\times l+1\to(i+1)\times l}^{k} \right] \end{pmatrix} \quad (13)$$

286 $$\widehat{y}_{i\times l+1\to(i+1)\times l}^{k} = h(x_{i+1}^{k-}, \vartheta_{i+1}^{k-}) \quad (14)$$

287 where ϑ_i is the parameter vector for sub-period i, represented as $\left(\theta_{i,1}, \theta_{i,2}, ..., \theta_{i,Np}\right)$;
288 x_i is the initial state vector for sub-period i; and l is the length of the sub-period.

289 This approach addresses the routing-lag issue by allowing parameters of the
290 routing processes, such as the instantaneous unit hydrograph, to remain constant for
291 each sub-period and to be time-varying over the whole period.

292 **2.4 Model evaluation criteria**

293 The streamflow simulations given by the proposed method are verified using the
294 NSE, relative error (RE) and NSE on logarithm of streamflow (NSE_{ln}) (Hock, 1999).
295 RE evaluates the error of the total volume of streamflow, while NSE and NSE_{ln}
296 evaluate the agreement between the hydrograph of observations and simulations. NSE
297 is more sensitive to high flows, but NSE_{ln} focuses more on low flows. Higher values

298 of NSE, NSE_{ln} and lower absolute values of RE indicate better streamflow simulations.

299 The NSE, RE and NSE_{ln} are expressed as followed:

300 $$NSE = 1 - \frac{\sum_{t=1}^{m}(Q_t - \widehat{Q}_t)^2}{\sum_{t=1}^{m}(Q_t - \overline{Q}_t)^2} \quad (15)$$

301 $$RE = \frac{\sum_{t=1}^{m}(Q_t - \widehat{Q}_t)}{\sum_{t=1}^{m}Q_t} \quad (16)$$

302 $$NSE_{\ln} = 1 - \frac{\sum_{t=1}^{m}(\ln(Q_t) - \ln(\widehat{Q}_t))^2}{\sum_{t=1}^{m}(\ln(Q_t) - \ln(\overline{Q}_t))^2}$$

303 The estimated parameters are evaluated by the RMSE (Alvisi et al., 2006), MARE
304 (Khalil et al., 2001) and R^2 (Kim et al., 2007) in the synthetic experiments (see details
305 in section 3.1). RMSE is more sensitive to high values than MARE, while R^2 is based
306 on the linear assumption (Dawson et al., 2007). Smaller values of RMSE, MARE and
307 higher values of R^2 indicate stronger parameter identification ability. For the *p*-th
308 parameter, the formulations are as follows:

309 $$RMSE_p = \sqrt{\frac{1}{m}\sum_{t=1}^{m}(\theta_{t,p} - \widehat{\theta}_{t,p})^2} \quad (18)$$

310 $$MARE_p = \frac{1}{m}\sum_{t=1}^{m}\frac{\left|\theta_{t,p} - \widehat{\theta}_{t,p}\right|}{\theta_{t,p}} \quad (19)$$

311 $$R^2_p = \frac{\sum_{t=1}^{m}\left(\widehat{\theta}_{t,p} - \overline{\widehat{\theta}}_p\right)\left(\theta_{t,p} - \overline{\theta}_p\right)}{\sqrt{\sum_{t=1}^{m}\left(\widehat{\theta}_{t,p} - \overline{\widehat{\theta}}_p\right)^2\left(\theta_{t,p} - \overline{\theta}_p\right)^2}} \quad (20)$$

where θ_t and $\widehat{\theta}_t$ are the true parameter and its estimated value at the *t*-th time step, respectively; $\overline{\theta}_p$ and $\overline{\widehat{\theta}}_p$ are the mean value of the true parameters and its estimated values, respectively; and m is the length of the data during the whole period.

3. Synthetic experiment and real catchment case study

Two synthetic experiments and two real catchment case studies were designed to assess the performance of SSC-DP. The experiments are described in Table 3.

3.1 Synthetic experiments

The two synthetic experiments examine the ability of SSC-DP to identify the time-varying parameters of the TMWB and Xinanjiang hydrological models. The merit of synthetic experiments is that the parameters can be synthetically generated to be either constant or time-varying. Hence, it is convenient to compare the estimated values with the pre-determined parameters to evaluate different parameter estimation methods. Note that synthetic experiments have been successfully used in several time-varying parameter identification studies (Deng et al., 2016; Pathiraja et al., 2016; Xiong et al., 2019).

3.1.1 Synthetic experiment with the TMWB model

Synthetic data of monthly precipitation and potential evapotranspiration were collected from the 03451500 catchment of the Model Parameter Estimation Experiment (MOPEX) (Duan et al., 2006). The data cover 252 months. Runoff was derived by the

TMWB model using synthetic precipitation, potential evapotranspiration, and the pre-determined parameters. Gaussian noise was added to the simulated runoff to represent uncertainties. The mean of the noise was set to zero, and the standard deviation was assumed to be 3 % of the magnitude of the values (Deng et al., 2016).

Eight scenarios with different pre-determined parameters were investigated (Table 4). The first scenario considered constant parameters. Scenarios 2 and 3 considered month-by-month variations in TMWB model parameters, i.e., the parameters remain constant during each month, but change from month to month. Scenarios 4 and 5 considered parameters that change every six months. Scenarios 6–8 considered year-by-year variations. The changes in both *C* and *SC* were considered to be linear in scenarios 2, 4, and 6 (Trend) and sinusoidal in scenarios 3, 5 and 7 (periodicity), reflecting the impacts of climate change and human activities (Pathiraja et al., 2016). Scenario 8 considered a periodic variation with an increasing trend for parameter *C* and only the linear variation in *SC*.

3.1.2 Synthetic experiment with the Xinanjiang model

Hourly precipitation and pan evaporation data were collected from the Baiyunshan Reservoir basin in China. The data cover a period of 18000 h. The Xinanjiang model has 15 parameters, which can lead to a significant computational burden. To reduce the total number of model runs, only the sensitive parameters were considered to be free. The Morris method was used to detect the free parameters (Fig. 4), with the results showing that *KE*, *CI*, *CG*, *KI*, *KG*, and *NK* are sensitive parameters. Thus, the other

353 parameters were held constant for the whole period.

354 Similar to the experiment with the TMWB model, the synthetic runoff was derived
355 from the Xinanjiang model with added Gaussian noise. The mean of the noise was set
356 to zero, and the standard deviation was assumed to be 5 % of the magnitude of the
357 values. As presented in Table 5, all 15 parameters were set to be constant in the first
358 scenario. The pre-determined sensitive parameters were considered to vary with a
359 certain trend and periodicity in scenarios 2 and 3, respectively. Scenario 4 considered a
360 combined variation of trend and periodicity for the parameter *KE*, with the other free
361 parameters set to vary linearly. The parameter variations in scenarios 2–4 were assumed
362 to occur once a month.

363 **3.2 Study area: Wuding River basin**

364 The Wuding River basin (Fig. 5(a)) examined in the first case study is a large sub-
365 basin of the Yellow River basin located on the Loess Plateau (Xu, 2011). The Wuding
366 River has a drainage area of 30261 km^2 and a total length of 491 km. The average slope
367 is 0.2 %, and the elevation varies from 600–1800 m above sea level. The area is a semi-
368 arid region with mean annual precipitation of ~401 mm. The annual potential
369 evapotranspiration is 1077 mm, and the mean annual runoff is 39 mm. The data for this
370 basin were collected over the period 1958–2000. The daily precipitation was obtained
371 from Thiessen polygons using records from 122 rain gauges. Based on meteorological
372 data from the China Meteorological Data Sharing Service System (http://data.cma.cn),
373 areal pan evaporation data were obtained. As illustrated in Fig. 5(a), the station furthest

downstream, Baijiachuan, drains an area of 29,662 km^2 (98 % of the total basin) and records the daily runoff data. The data of the daily precipitation and streamflow in the Wuding River basin were obtained from the local Hydrology and Water Resources Bureau of China, the quality of which has been checked by the official authorities, and there are no gaps among these data for all the hydrological stations. It can be seen from Fig. 5(c) that the annual streamflow in the Wudinghe River basin has a distinct decreasing trend, while seasonal variations are not significant, but the annual precipitation and pan evaporation generally have no trend, suggesting the impacts of human activities on rainfall-runoff relationships.

Soil and water conservation measures, such as the construction of the check dams and afforestation, have been undertaken since the 1960s. The areas of two soil and water conservation measures are plotted in Fig. 5(e), the data of which were collected from Zhang et al. (2002). The areas of tree planting have an increasing trend, but the slope gets much larger after 1972. It indicates that greater efforts have been made for afforestation since the turning point. Similarly, the areas of dammed lands also increase, but the rate gets slower after 1972. These two soil and water conservation measures had changed the underlying surface of the watershed and impacted the relationship between precipitation and runoff (Gao et al., 2017; Jiao et al., 2017).

3.3 Study area: Xun River basin

The proposed method was also applied to the Xun River basin, China (Fig. 5(b)). Located between 108°24’–109°26’ E and 32°52’–33°55’ N, the study area covers

approximately 6448 km^2. The Xun River is ~218 km long and has an average annual flow of 73 m^3/s (Li et al., 2016). The basin has a subtropical monsoon climate. The weather is wet and moderate with an annual average temperature of 15–17 °C. The daily hydrological data from 1991–2001 include precipitation from 28 rainfall stations, pan evaporation from three hydrological gauged stations, and discharge at the outlet of the Xun River basin. Areal precipitation was obtained using the Thiessen polygon method, and areal pan evaporation was computed using the average value of the data from gauged stations. The data in the Xun River basin were also obtained from the local Hydrology and Water Resources Bureau of China, and there are no gaps among these data for all the hydrological stations.

It can be observed from Fig. 5(d) that no trend is found in annual precipitation, pan evaporation and streamflow, suggesting that the relationship between precipitation and runoff of the Xun River basin is rarely affected by human activities during 1991-2001. However, there exhibit strong seasonal patterns in these three climatic and hydrological variables, suggesting that seasonal variations in hydrological parameters should be considered.

4. Results

4.1 Synthetic experiment

4.1.1 Results of synthetic experiment with the TMWB model

When using SSC-DP, the first task is to define how the hydrological data series should be split into the k sub-periods within which the parameters are assumed to be

416 constant. As climate change can induce seasonal or half-annual variations while human
417 activities usually influence the watershed annually, lengths of three months, six months,
418 and 12 months were arbitrarily chosen. Thus, this experiment compared the following
419 four methods: (1) EnKF; (2) 3-SSC-DP; (3) 6-SSC-DP, and (4) 12-SSC-DP.

420 Figure 6(a) presents the runoff simulation performance for various scenarios. In
421 scenario 1, the NSE values of the three SSC-DP methods are all higher than that of
422 EnKF. The results of NSE_{ln} show no significant differences among various methods.
423 For scenarios 2, 4, and 6, where true parameters have linear trends, the 6-SSC-DP and
424 12-SSC-DP are superior to the EnKF and 3-SSC-DP in terms of NSE and NSE_{ln}. In
425 scenario3, where the true parameters have periodic variations and change every month,
426 the NSE and NSE_{ln} values of 6-SSC-DP and 12-SSC-DP decrease significantly,
427 because the assumed sub-period length is longer than the time-scale of actual variations.
428 Similarly, in scenario 5, 12-SSC-DP performs worst for NSE and NSE_{ln}, but 6-SSC-
429 DP performs best. In scenario 7 and 8, both 6-SSC-DP and 12-SSC-DP perform better
430 than EnKF. According to the evaluations of NSE and NSE_{ln}, the SSC-DP offers
431 improved accuracy than the EnKF if the proper length is chosen. Another advantage of
432 the SSC-DP is the small RE. For all scenarios, the SSC-DP methods significantly
433 outperform for RE compared with EnKF. Among the SSC-DP methods, the RE of 3-
434 SSC-DP is the smallest.

435 Figures 6 (b) and (c) focuses on the ability of the four methods to identify time-
436 varying parameters. It can be seen that the RMSE and MARE values of the 3-SSC-DP
437 are larger than those of other methods in most cases. That is because the sub-period

438 length that serves as a calibration period for MCMC is too short (i.e., three months) that
439 the estimated parameters are associated with higher uncertainties.

440 Regarding the synthetic true parameters are constant values (scenario 1), 12-SSC-
441 DP gives the best performance with the lowest RMSE, MARE and highest R^2. The
442 observations and estimated parameters are presented in Figure 7 (b). It shows that the
443 estimated parameters obtained by EnKF vary at every time step, resulting in larger
444 deviations from the observations than 6-SSC-DP and 12-SSC-DP.

445 When the synthetic true parameters vary linearly (scenarios 2, 4, and 6), 12-SSC-
446 DP produces the best estimations in comparison with EnKF, 3-SSC-DP, and 6-SSC-
447 DP. The performances of 6-SSC-DP and EnKF are similar.

448 When the synthetic true parameters vary sinusoidally from month to month, EnKF
449 gives the best estimations in scenario 3. The poor performances of 6-SSC-DP and 12-
450 SSC-DP can be explained by the sub-period length being much longer than the actual
451 one. When the parameters vary periodically at six-month intervals (scenario 5), 6-SSC-
452 DP yields the best performance with the lowest RMSE, MARE and highest R^2. The
453 differences in estimation performances among 3-SSC-DP, 12-SSC-DP and EnKF are
454 small. The estimated parameters for scenario 5 have been plotted in Fig. 7(a). Although
455 3-SSC-DP and 12-SSC-DP have different lengths of sub-periods, they can also detect
456 the correct seasonal signal of the parameters. For the annual variation in parameters
457 (scenario 7), 12-SSC-DP and 6-SSC-DP produce better results than EnKF. Similar
458 results can be seen in scenario 8 where C has a combined variation from year to year.
459 In summary, the results indicate that the SSC-DP with a suitable length can estimate

460 more accurate parameters than EnKF.

461 **4.1.2 Results of synthetic experiment with the Xinanjiang model**

462 The Xinanjiang model is more complex than TMWB, and so some sensitivity
463 analysis is necessary. As stated in Sect. 3.1.2, the sensitive parameters are *KE*, *CI*, *CG*,
464 *KI*, *KG*, and *NK*. The 18000 hourly hydrological data points were divided into 25 sub-
465 periods (monthly time scale) and 12 sub-periods (bimonthly time scale). It is considered
466 that a monthly time scale helps diagnose seasonal variations, whereas a two-monthly
467 time scale provides data for longer calibration lengths.

468 Three data assimilation methods (see Sect. 2.3.2 for details) were applied to the
469 synthetic data: (1) EnKF; (2) EnKS, and (3) SSC-EnKF. The results in Fig. 8 indicate
470 that EnKS is superior to EnKF, as previously observed (Li et al., 2013), although SSC-
471 EnKF gives the best results. This is probably because SSC-EnKF is based on the
472 assumption that the parameters remain constant during each sub-period.

473 The simulated streamflow and identification of time-varying parameters were
474 compared across four methods: 1-SSC, SSC-EnKF, 1-SSC-DP, and 2-SSC-DP. The
475 simulation performance is summarized in Figure 9(a). For all scenarios, the NSE of 2-
476 SSC-DP is the lowest, but it performs better for low flows. The SSC-EnKF produces
477 the highest RE in scenarios 2, 3 and 4, indicating the problem of simulating water
478 balance. The SSC and 1-SSC-DP perform well for all scenarios in terms of NSE, RE
479 and NSE_{ln}. Wherein, the SSC performs better than the 1-SSC-DP with regard to RE,
480 while 1-SSC-DP is slightly superior to SSC in scenario 3 with higher NSE_{ln}.

481 Figures 9(b) and (c) compare the time-varying parameter estimation performance
482 among the four methods. In scenarios 1 and 2, 2-SSC-DP produces the lowest RMSE,
483 MARE and R^2, followed by the 1-SSC-DP. The 1-SSC-DP is slightly superior to the 1-
484 SSC and significantly outperforms the SSC-EnKF for the two scenarios.
485 When the synthetic true parameters vary sinusoidally from month to month
486 (scenario 3), the estimated parameters are plotted in Fig. 10. It can be seen that 1-SSC-
487 DP successfully detects a seasonal signal in every parameter. The SSC-EnKF performs
488 well for R^2, but it has high MARE. Although the average MARE of the SSC and 2-
489 SSC-DP are lower than that of SSC-EnKF, the R^2 of them are relatively low. Therein,
490 from Fig. 10, the estimated parameters by the 1-SSC fluctuate generally periodically,
491 but the variations are dramatic, resulting in the lowest R^2 for CI, KI, KG and NK. The
492 estimated parameters of the 2-SSC-DP fluctuate more slowly, but the sub-period length
493 is too long. In scenario 4, 1-SSC performs better than the SSC-EnKF and 2-SSC-DP,
494 but is still slightly inferior to the 1-SSC-DP. Overall, the 1-SSC-DP achieves higher-
495 quality and more robust parameter estimations performances than the other methods.

496 **4.2 Case study: Wuding River basin**

497 Figures 11(a) and (b) show the double mass curves between daily runoff and
498 precipitation for the Wuding River basin. Similar to the work of Deng et al. (2016), the
499 two linear slopes (p-value < 0.05) of the curves are different before and after 1972,
500 demonstrating the relationship between precipitation and runoff changes under the soil
501 and water conservation measures. This suggests that there are annual variations in the

502 watershed characteristics. Hence, the length of each sub-period was set to 12 months,
503 and the time-varying parameters were identified using 12-SSC-DP. Based on daily
504 Wuding data from 1958–2000, sensitivity analysis showed that nine parameters of the
505 Xinanjiang model are relatively sensitive: *WM*, *WUM*, *WLM*, *KE*, *IMP*, *KI*, *KG*, *N*, and
506 *NK*.

507 The simulation results given by 12-SSC-DP were benchmarked against those from
508 12-SSC, data assimilation, and the conventional method in which all Xinanjiang model
509 parameters remain constant. The simulation performance is presented in Figure 12. The
510 values of the NSEs are relatively low, because the streamflow in dry regions is difficult
511 to simulate. It can be seen that the 12-SSC-DP gives the best simulation results among
512 different methods with the highest NSE, NSE_{ln} and small RE. Although the 12-SSC
513 produces relatively high NSE, it performs the worst simulations for low flows. The
514 SSC-EnKF has relatively high NSE_{ln}, but the RE of it is the largest. Overall, the 12-
515 SSC-DP significantly improves the simulation performance of the Xinanjiang model in
516 the Wuding River basin.

517 Although the objective function of 12-SSC-DP considers the trade-off between
518 simulation accuracy and parameter continuity, 12-SSC-DP gives a higher NSE value.
519 This may be because 12-SSC locates a local peak over one sub-period, resulting in
520 unreasonable model states for the beginning of the next sub-period, whereas 12-SSC-
521 DP uses dynamic programming to explore more reasonable parameter values and model
522 states. Figure 13 shows the quantile-quantile plots, from which it can be seen that if the
523 parameters are assumed to be constant, streamflow is highly underestimated. The

underestimation mainly derives from the deficiencies of the model structure. Methods 12-SSC and 12-SSC-DP reduce this underestimation by using time-varying parameters. Additionally, 12-SSC-DP is slightly inferior to 12-SSC in terms of peak flows, but is superior in terms of simulating streamflow lower than 100 m^3/s, which accounts for 80 % of the whole streamflow time series. It can be inferred that the 12-SSC-DP is more applicable to the simulation of streamflow in the Wuding River basin.

The estimated time-varying parameters estimated by 12-SSC-DP are plotted in Fig.14. The results show that *WM* remains constant before and after 1972, but *WUM* varies significantly over this period, indicating that the distribution of soil water capacity may change, i.e., *WUM* decreases but *WLM* increases. A Person correlation analysis is applied to investigate the relationship between the areas of tree planting and *WUM* as well as *WLM*. It is found that there is a significant negative correlation (Pearson correlation efficient ρ=-0.38, P<0.05) between the areas of tree planting and *WUM*. While *WLM* has a nonsignificant positive correlation (ρ=0.26, P>0.05) with the areas of tree planting. It can be inferred that less severe soil erosion occurred, because the upper layers became thinner while the lower layer, where vegetation roots dominate, became thicker (Jayawardena and Zhou, 2000). Additionally, *IMP* is significantly correlated with the areas of tree planting (ρ=-0.33, P<0.05). Except for afforestation, the areas of the dammed lands are significantly correlated with *WLM* (ρ=0.46, P<0.05), suggesting that the construction of the check dams also has an influence on the soil water capacity of the Wuding river basin. Other parameters, *KE*, *KI*, *KG*, *N* and *NK* have little differences before and after 1972. The variations in *WLM* and *IMP* slowed

546 down after the turning point, similar to the results of Deng et al. (2016).

547 **4.3 Case study: Xun River basin**

548 Figures 11(c) and (d) show the double mass curves between runoff and
549 precipitation for the Xun River basin. The linear slope of the curve is generally
550 stationary for the whole ten-year period shown in Fig. 11(c), with a correlation
551 coefficient of 99.6 %. In contrast, the linear slope for an intra-annual timescale is non-
552 stationary (Fig. 11(d)). Based on these results, it can be inferred that the relationship
553 between precipitation and runoff is stable from 1990–2000, but varies over the intra-
554 annual timescale. Hence, sub-periods of three and 12 months were examined in the Xun
555 River basin using models 3-SSC-DP and 12-SSC-DP. From the Xun River basin data
556 from 1991–2000, sensitivity analysis suggested that five parameters of the Xinanjiang
557 model are relatively sensitive, namely *KE*, *B*, *KI*, *KG*, and *NK*.

558 Similar to the case study of the Wuding River basin, the simulation performance
559 of 3-SSC-DP was benchmarked against that of 3-SSC, data assimilation, and the
560 conventional calibration method. Among the data assimilation methods described in
561 Sect. 2.3.2, 3-SSC-EnKF gives the highest simulation accuracy. The simulation
562 performance is presented in Figure 15. All methods performed well, with NSE values
563 of 92.5 %, 93.0 %, 95.0 %, and 94.8 % for the conventional method, 3-SSC-EnKF, 3-
564 SSC, and 3-SSC-DP, respectively. 3-SSC and 3-SSC-DP also perform well for NSE_{ln}
565 compared with 3-SSC-EnKF and the conventional method. However, as regards to RE,
566 the values are 0.0007 and 0.0324 for 3-SSC-DP and 3-SSC-DP, respectively. It

567 indicated that the 3-SSC-DP can better simulate water balance than the 3-SSC in the
568 Xun River basin. Figure 16 illustrates the hydrograph and quantile-quantile plots for
569 the simulations in the Xun river basin. It is evident that the peak flows estimated by the
570 3-SSC are higher than those of 3-SSC-DP, and 3-SSC-DP simulate better the flows
571 ranging from 100 m^3/s to 200 m^3/s.

572 The estimated parameters using 3-SSC-DP are presented in Fig. 17(a). Some
573 parameters vary significantly over an intra-annual time scale. Among them, the
574 parameter *KE*, representing the ratio of potential evapotranspiration to pan evaporation,
575 exhibits the most distinct seasonal variations. A fast Fourier transform was used to
576 calculate the spectral power of the *KE* time series to explore its periodic characteristics.
577 As can be observed from Fig. 17(b), 3-SSC-DP had the greatest spectral power, for a
578 period of 4.0 cycles per year, somewhat higher than the power obtained by 3-SSC and
579 3-SSC-EnKF. This means a stronger periodic pattern is captured by 12-SSC-DP. Given
580 that the estimated *KE* varies at three-monthly intervals, it has a one-year periodicity.
581 The other parameters do not exhibit significant one-year periodic patterns. This may be
582 because only *KE*, linking potential evapotranspiration and pan evaporation, is directly
583 impacted by seasonal climate variations, such as temperature.

584 ## 5. Discussion

585 As noted in the methodology section, the performance of the proposed method is
586 influenced by several factors, such as the weights in the objective function and the
587 choice of lengths. Some suggestions regarding the improvement of the proposed
588 approach are now discussed in detail.

589 **5.1 Objective function of dynamic programming in SSC-DP**

590 In the conventional method, a parameter set is identified as optimal for providing
591 the best simulation over the calibration period. However, other parameter sets with
592 slightly worse (but still good) performance can also be candidates. Allowing for input
593 data uncertainty and local optima, SSC-DP identifies parameter sets that perform near-
594 optimally and display fewer fluctuations over sub-periods. This can be adjusted by
595 weights in the objective function of the dynamic programming approach (see Eq. (3)).
596 As the weighting for accuracy increases, parameters providing more accurate
597 simulations are chosen, but parameter continuity is less important. If too much
598 importance is given to continuity, the variations in real-world processes may be
599 underestimated. Here, the influence of different weights has been assessed for
600 simulation accuracy and parameter continuity based on synthetic experiments with the
601 TMWB and Xinanjiang models, respectively. Specifically, the weight for simulation
602 accuracy was set to 1, and the weight for parameter continuity α varied from zero to a
603 small positive value (e.g., 1). When $\alpha = 0$, only simulation accuracy was considered.

604 Figure 18(a) shows the R^2 value of 12-SSC-DP with various continuity weights for
605 scenario 4 in the synthetic experiment with the TMWB model. It can be seen that R^2 is
606 lowest when $\alpha = 0$ for both *C* and *SC*. There is some improvement when a nonzero
607 weight is applied. As α increases, the performance of 12-SSC-DP improves, and then
608 worsens; the differences among schemes with nonzero weights are not distinct. Similar
609 results can be observed in Fig. 18(b), which presents the R^2 value of 12-SSC-DP with
610 various α for scenario 2 in the synthetic experiment with the Xinanjiang model.

611 Therefore, nonzero continuity weights can significantly improve the parameter
612 estimation performance compared with the zero-weight case. It is suggested that
613 weights of 1 (accuracy) and 0.005 (continuity) be used with the TMWB model and
614 weights of 1 (accuracy) and 0.2 (continuity) be applied with the Xinanjiang model, as
615 in this study.

616 **5.2 Choice of sub-period length in SSC-DP**

617 As mentioned by Gharari et al. (2013), there are different ways of determining the
618 sub-period lengths. The sub-periods can be non-continuous hydrological years (Seiller
619 et al., 2012), months or seasons (Deng et al., 2018; Paik et al., 2005), and discharge or
620 precipitation events (Singh and Bardossy, 2012). This introduces a controversial issue
621 whereby parameters are impacted by the length of the calibration period. Merz et al.
622 (2009) suggested that 3–5 years is an acceptable calibration period, whereas Singh and
623 Bardossy (2012) indicated that a small number of events may be sufficient for
624 parameter identification. It is suggested that the determination of the sub-period length
625 considers three factors:

626 (1) The temporal scale of climate change or human activities. For example, the
627 Wudinghe River basin is taken as a case study. The soil and water conservation
628 measures have led to a durative and long-term change in the catchment characteristic
629 since the 1960s. Due to this, the yearly sub-period is preferred.

630 (2) The seasonality. Contrary to the Wudinghe River basin, the relationship
631 between precipitation and runoff of the Xun River basin is rarely affected by human

activities during 1991-2001. However, its significant seasonal dynamics can be observed and has been studied in the literature (Lan et al., 2020; Lan et al., 2018). In order to diagnose the seasonality, the stable period of 3-month is adopted.

(3) The simulation accuracy. The length should be neither too long nor too short so as to increase the reliability of the calibration while guaranteeing that variations in real processes are captured. Thus, given that the time scale of the variations is unknown, the proposed SSC-DP can be used with different split-sample lengths. It is suggested that the length should be as long as possible without degrading the simulation performance significantly. For example, in the synthetic experiment with the TMWB model, if the difference between the NSE values of 6-SSC-DP and 3-SSC-DP is small, the preferred length is 6-month.

However, many studies are based on the conventional assumption that the parameters of different sub-periods are independent. Hence, the sub-period lengths should be long enough to reduce the degree of uncertainty. In this study, the assumption of parameter continuity is introduced to give another constraint that considers correlations between parameters of adjacent sub-periods. It appears that the determination of sub-period lengths deserves further investigation.

6. Conclusions

This paper has described a time-varying parameter estimation approach based on dynamic programming. The proposed SSC-DP combines the basic concept of SSC and the continuity assumption of data assimilation to estimate more continuous parameters while providing comparably good streamflow simulations. Two synthetic experiments

were designed to evaluate its applicability and efficiency for time-varying parameter identification. Furthermore, two case studies were conducted to explore the advantages of SSC-DP in real catchments. From the results, the following conclusions can be drawn:

1. The proposed method with a suitable length not only produces better simulation performance, but also ensures more accurate parameter estimates than SSC and EnKF in the synthetic experiment using the TMWB model with two parameters. The impact of sub-period lengths on the performance of SSC-DP is significant when the pre-determined parameters vary sinusoidally.

2. The proposed method can be used to deal with complex hydrological models involving a large number of parameters, demonstrated by the synthetic experiment using the Xinanjiang model with 15 parameters. A sensitivity analysis was performed to reduce the probable computational cost and improve the efficiency of identifying the time-varying parameters.

3. The proposed method has the potential to detect the relationship between the time-varying parameters and dynamic catchment characteristics. For example, SSC-DP produces the best simulation performance in the case study of the Wuding River basin and detects that parameters representing soil water capacity and impervious areas changed significantly after 1972, reflecting the soil and water conservation projects carried out from 1958–2000. Additionally, SSC-DP detects the strongest seasonal signal in the case study of Xun River basin, indicating the distinct impacts of seasonal climate variability.

This study has demonstrated that the proposed method is an effective approach for

identifying time-varying parameters under changing environments. Further work is still needed, such as to determine an objective method for choosing the sub-period lengths.

Acknowledgements

This study was supported by the Natural Science Foundation of Hubei Province (2017CFA015), the National Natural Science Foundation of China (51861125102), and Innovation Team in Key Field of the Ministry of Science and Technology (2018RA4014). The authors would like to thank the editor and anonymous reviewers for their comments that helped improve the quality of the paper.

Code/Data availability

The data and codes that support the findings of this study are available from the corresponding author upon request.

Author contribution

All of the authors helped to develop the method, designed the experiments, analyzed the results and wrote the paper.

Compliance with Ethical Standards

Conflict of Interest The authors declare that they have no conflict of interest.

References

Alvisi, S., Mascellani, G., Franchini, M., Bardossy, A., 2006. Water level forecasting through fuzzy logic and artificial neural network approaches. Hydrology and Earth System Sciences 10(1), 1-17.

Bellman, R., 1957. Dynamic programming. Princeton University Press, Princeton.

Broderick, C., Matthews, T., Wilby, R.L., Bastola, S., Murphy, C., 2016. Transferability of hydrological models and ensemble averaging methods between contrasting climatic periods. Water Resources Research 52(10), 8343-8373.

Bronstert, A., 2004. Rainfall-runoff modelling for assessing impacts of climate and land-use change. Hydrological Processes 18(3), 567-570.

Chen, Y., Zhang, D., 2006. Data assimilation for transient flow in geologic formations via ensemble kalman filter. Advances in Water Resources 29(8), 1107-1122.

Chib, S., Greenberg, E., 1995. Understanding the metropolis-hastings algorithm. American Statistician 49(4), 327-335.

Coron, L. et al., 2012. Crash testing hydrological models in contrasted climate conditions: An experiment on 216 australian catchments. Water Resources Research 48.

Dai, C., Qin, X.S., Chen, Y., Guo, H.C., 2018. Dealing with equality and benefit for water allocation in a lake watershed: A gini-coefficient based stochastic optimization approach. Journal of Hydrology 561, 322-334.

Dawson, C.W., Abrahart, R.J., See, L.M., 2007. Hydrotest: A web-based toolbox of evaluation metrics for the standardised assessment of hydrological forecasts. Environmental Modelling & Software 22(7), 1034-1052.

Deng, C., Liu, P., Guo, S., Li, Z., Wang, D., 2016. Identification of hydrological model parameter variation using ensemble kalman filter. Hydrology and Earth System Sciences 20(12), 4949-4961.

Deng, C., Liu, P., Wang, D., Wang, W., 2018. Temporal variation and scaling of parameters for a monthly hydrologic model. Journal of Hydrology 558, 290-300.

Deng, C., Liu, P., Wang, W., Shao, Q., Wang, D., 2019. Modelling time-variant parameters of a two-parameter monthly water balance model. Journal of Hydrology 573, 918-936.

Duan, Q. et al., 2006. Model parameter estimation experiment (mopex): An overview of science strategy and major results from the second and third workshops. Journal of Hydrology 320(1-2), 3-17.

Feng, M. et al., 2017. Deriving adaptive operating rules of hydropower reservoirs using time-varying parameters generated by the enkf. Water Resources Research 53(8), 6885-6907.

Fowler, K., Peel, M., Western, A., Zhang, L., 2018. Improved rainfall-runoff calibration for drying climate: Choice of objective function. Water Resources Research 54(5), 3392-3408.

Fowler, K.J.A., Peel, M.C., Western, A.W., Zhang, L., Peterson, T.J., 2016. Simulating runoff under changing climatic conditions: Revisiting an apparent deficiency of conceptual rainfall-runoff models. Water Resources Research 52(3), 1820-1846.

Gao, S. et al., 2017. Derivation of low flow frequency distributions under human activities and its implications. Journal of Hydrology 549, 294-300.

Gharari, S., Hrachowitz, M., Fenicia, F., Savenije, H.H.G., 2013. An approach to identify time consistent model parameters: Sub-period calibration. Hydrology and Earth System Sciences 17(1), 149-161.

Guo, S.L., Wang, J.X., Xiong, L.H., Ying, A.W., Li, D.F., 2002. A macro-scale and semi-distributed monthly water balance model to predict climate change impacts in china. Journal of Hydrology 268(1-

4), 1-15.
Guzha, A.C., Rufino, M.C., Okoth, S., Jacobs, S., Nobrega, R.L.B., 2018. Impacts of land use and land cover change on surface runoff, discharge and low flows: Evidence from east africa. Journal of Hydrology-Regional Studies 15, 49-67.
Hock, R., 1999. A distributed temperature-index ice- and snowmelt model including potential direct solar radiation. Journal of Glaciology 45(149), 101-111.
Hughes, D.A., 2015. Simulating temporal variability in catchment response using a monthly rainfall-runoff model. Hydrological Sciences Journal-Journal Des Sciences Hydrologiques 60(7-8), 1286-1298.
Hundecha, Y., Bardossy, A., 2004. Modeling of the effect of land use changes on the runoff generation of a river basin through parameter regionalization of a watershed model. Journal of Hydrology 292(1-4), 281-295.
Jayawardena, A.W., Zhou, M.C., 2000. A modified spatial soil moisture storage capacity distribution curve for the xinanjiang model. Journal of Hydrology 227(1-4), 93-113.
Jeremiah, E., Marshall, L., Sisson, S.A., Sharma, A., 2013. Specifying a hierarchical mixture of experts for hydrologic modeling: Gating function variable selection. Water Resources Research 49(5), 2926-2939.
Jiao, Y. et al., 2017. Impact of vegetation dynamics on hydrological processes in a semi-arid basin by using a land surface-hydrology coupled model. Journal of Hydrology 551, 116-131.
Jie, M.X. et al., 2018. Transferability of conceptual hydrological models across temporal resolutions: Approach and application. Water Resources Management 32(4), 1367-1381.
Khalil, M., Panu, U.S., Lennox, W.C., 2001. Groups and neural networks based streamflow data infilling procedures. Journal of Hydrology 241(3-4), 153-176.
Kim, S., Hong, S.J., Kang, N., Noh, H.S., Kim, H.S., 2016. A comparative study on a simple two-parameter monthly water balance model and the kajiyama formula for monthly runoff estimation. Hydrological Sciences Journal-Journal Des Sciences Hydrologiques 61(7), 1244-1252.
Kim, S.M., Benham, B.L., Brannan, K.M., Zeckoski, R.W., Doherty, J., 2007. Comparison of hydrologic calibration of hspf using automatic and manual methods. Water Resources Research 43(1).
Kim, S.S.H., Hughes, J.D., Chen, J., Dutta, D., Vaze, J., 2015. Determining probability distributions of parameter performances for time-series model calibration: A river system trial. Journal of Hydrology 530, 361-371.
King, D.M., Perera, B.J.C., 2013. Morris method of sensitivity analysis applied to assess the importance of input variables on urban water supply yield - a case study. Journal of Hydrology 477, 17-32.
Klemes, V., 1986. Operational testing of hydrological simulation-models. Hydrological Sciences Journal-Journal Des Sciences Hydrologiques 31(1), 13-24.
Lan, T., Lin, K., Xu, C.-Y., Tan, X., Chen, X., 2020. Dynamics of hydrological-model parameters: Mechanisms, problems and solutions. Hydrology and Earth System Sciences 24(3), 1347-1366.
Lan, T. et al., 2018. A clustering preprocessing framework for the subannual calibration of a hydrological model considering climate-land surface variations. Water Resources Research 54(0).
Li, H. et al., 2018. Hybrid two-stage stochastic methods using scenario-based forecasts for reservoir refill operations. Journal of Water Resources Planning and Management 144(12).
Li, H., Zhang, Y., 2017. Regionalising' rainfall-runoff modelling for predicting daily runoff: Comparing gridded spatial proximity and gridded integrated similarity approaches against their lumped counterparts. Journal of Hydrology 550, 279-293.

784 Li, Y., Ryu, D., Western, A.W., Wang, Q.J., 2013. Assimilation of stream discharge for flood forecasting:
785 The benefits of accounting for routing time lags. Water Resources Research 49(4), 1887-1900.
786 Li, Z. et al., 2016. Evaluation of estimation of distribution algorithm to calibrate computationally
787 intensive hydrologic model. Journal of Hydrologic Engineering 21(6).
788 Lin, K. et al., 2014. Xinanjiang model combined with curve number to simulate the effect of land use
789 change on environmental flow. Journal of Hydrology 519, 3142-3152.
790 Lu, H. et al., 2013. The streamflow estimation using the xinanjiang rainfall runoff model and dual state-
791 parameter estimation method. Journal of Hydrology 480, 102-114.
792 Luo, M., Pan, C., Zhan, C., 2019. Diagnosis of change in structural characteristics of streamflow series
793 based on selection of complexity measurement methods: Fenhe river basin, china. Journal of
794 Hydrologic Engineering 24(2).
795 Meng, S., Xie, X., Liang, S., 2017. Assimilation of soil moisture and streamflow observations to improve
796 flood forecasting with considering runoff routing lags. Journal of Hydrology 550, 568-579.
797 Merz, R., Parajka, J., Bloeschl, G., 2009. Scale effects in conceptual hydrological modeling. Water
798 Resources Research 45.
799 Merz, R., Parajka, J., Bloeschl, G., 2011. Time stability of catchment model parameters: Implications for
800 climate impact analyses. Water resources research 47(W02531).
801 Ming, B., Liu, P., Bai, T., Tang, R., Feng, M., 2017. Improving optimization efficiency for reservoir
802 operation using a search space reduction method. Water Resources Management 31(4), 1173-
803 1190.
804 Moradkhani, H., Sorooshian, S., Gupta, H.V., Houser, P.R., 2005. Dual state-parameter estimation of
805 hydrological models using ensemble kalman filter. Advances in Water Resources 28(2), 135-
806 147.
807 Morris, M.D., 1991. Factorial sampling plans for preliminary computational experiments. Technometrics
808 33(2), 161-174.
809 Nash, J.E., Sutcliffe, J.V., 1970. River flow forecasting through conceptual models part i — a discussion
810 of principles. Journal of Hydrology 10(3), 282-290.
811 Paik, K., Kim, J.H., Kim, H.S., Lee, D.R., 2005. A conceptual rainfall-runoff model considering seasonal
812 variation. Hydrological Processes 19(19), 3837-3850.
813 Pappenberger, F., Beven, K.J., Ratto, M., Matgen, P., 2008. Multi-method global sensitivity analysis of
814 flood inundation models. Advances in Water Resources 31(1), 1-14.
815 Pathiraja, S. et al., 2018. Time-varying parameter models for catchments with land use change: The
816 importance of model structure. Hydrology and Earth System Sciences 22(5), 2903-2919.
817 Pathiraja, S., Marshall, L., Sharma, A., Moradkhani, H., 2016. Hydrologic modeling in dynamic
818 catchments: A data assimilation approach. Water Resources Research 52(5), 3350-3372.
819 Poulin, A., Brissette, F., Leconte, R., Arsenault, R., Malo, J.-S., 2011. Uncertainty of hydrological modelling
820 in climate change impact studies in a canadian, snow-dominated river basin. Journal of
821 Hydrology 409(3-4), 626-636.
822 Quoc Quan, T., De Niel, J., Willems, P., 2018. Spatially distributed conceptual hydrological model building:
823 A genetic top-down approach starting from lumped models. Water Resources Research 54(10),
824 8064-8085.
825 Rebolho, C., Andreassian, V., Le Moine, N., 2018. Inundation mapping based on reach-scale effective
826 geometry. Hydrology and Earth System Sciences 22(11), 5967-5985.
827 Refsgaard, J.C., Knudsen, J., 1996. Operational validation and intercomparison of different types of

828 hydrological models. Water Resources Research 32(7), 2189-2202.
829 Seiller, G., Anctil, F., Perrin, C., 2012. Multimodel evaluation of twenty lumped hydrological models
830 under contrasted climate conditions. Hydrology and Earth System Sciences 16(4), 1171-1189.
831 Si, W., Bao, W., Gupta, H.V., 2015. Updating real-time flood forecasts via the dynamic system response
832 curve method. Water Resources Research 51(7), 5128-5144.
833 Singh, S.K., Bardossy, A., 2012. Calibration of hydrological models on hydrologically unusual events.
834 Advances in Water Resources 38, 81-91.
835 Siriwardena, L., Finlayson, B.L., McMahon, T.A., 2006. The impact of land use change on catchment
836 hydrology in large catchments: The comet river, central queensland, australia. Journal of
837 Hydrology 326(1-4), 199-214.
838 Sobol, I.M., 1993. Sensitivity estimates for nonlinear mathematical models. Mathematical modelling
839 and computational experiments 1(4), 407-414.
840 Stephens, C.M., Marshall, L.A., Johnson, F.M., 2019. Investigating strategies to improve hydrologic
841 model performance in a changing climate. Journal of Hydrology 579.
842 Sun, Y. et al., 2018. Development of multivariable dynamic system response curve method for real-time
843 flood forecasting correction. Water Resources Research 54(7), 4730-4749.
844 Teweldebrhan, A.T., Burkhart, J.F., Schuler, T.V., 2018. Parameter uncertainty analysis for an operational
845 hydrological model using residual-based and limits of acceptability approaches. Hydrology and
846 Earth System Sciences 22(9), 5021-5039.
847 Thirel, G. et al., 2015. Hydrology under change: An evaluation protocol to investigate how hydrological
848 models deal with changing catchments. Hydrological Sciences Journal-Journal Des Sciences
849 Hydrologiques 60(7-8), 1184-1199.
850 Toth, E., Brath, A., 2007. Multistep ahead streamflow forecasting: Role of calibration data in conceptual
851 and neural network modeling. Water Resources Research 43(11).
852 Westra, S., Thyer, M., Leonard, M., Kavetski, D., Lambert, M., 2014. A strategy for diagnosing and
853 interpreting hydrological model nonstationarity. Water Resources Research 50(6), 5090-5113.
854 Xie, S. et al., 2018. A progressive segmented optimization algorithm for calibrating time-variant
855 parameters of the snowmelt runoff model (srm). Journal of Hydrology 566, 470-483.
856 Xiong, L.H., Guo, S.L., 1999. A two-parameter monthly water balance model and its application. Journal
857 of Hydrology 216(1-2), 111-123.
858 Xiong, M. et al., 2019. Identifying time-varying hydrological model parameters to improve simulation
859 efficiency by the ensemble kalman filter: A joint assimilation of streamflow and actual
860 evapotranspiration. Journal of Hydrology 568, 758-768.
861 Xu, J., 2011. Variation in annual runoff of the wudinghe river as influenced by climate change and human
862 activity. Quaternary International 244(2), 230-237.
863 Yang, N. et al., 2017. Evaluation of the trmm multisatellite precipitation analysis and its applicability in
864 supporting reservoir operation and water resources management in hanjiang basin, china.
865 Journal of Hydrology 549, 313-325.
866 Yang, X. et al., 2018. A new fully distributed model of nitrate transport and removal at catchment scale.
867 Water Resources Research 54(8), 5856-5877.
868 Yin, J. et al., 2018. A copula-based analysis of projected climate changes to bivariate flood quantiles.
869 Journal of Hydrology 566, 23-42.
870 Zhang, J., Ji, W., Feng, X., 2002. Water and sediment changes in the wudinghe river: Present state,
871 formative cause and tendency in the future. A study of water and sediment changes in the

872 Yellow River 2, 393-429.
873 Zhao, R.J., 1992. The xinanjiang model applied in china. Journal of Hydrology 135(1-4), 371-381.
874

Table 1 Parameters of the TMWB model

Parameter	Physical meaning	Range and units
C	Evapotranspiration parameter	0.2-2.0 (–)
SC	Catchment water storage capacity	100-2000 (mm)

Table 2 Parameters of the Xinanjiang model

Category	Parameter	Physical meaning	Range and units
Evapotranspiration	WM	Tension water capacity	80-400 (mm)
	X	WUM=X×WM, WUM is the tension water capacity of lower layer	0.01-0.8 (–)
	Y	WLM=Y×WM, WLM is the tension water capacity of deeper layer	0.01-0.8 (–)
	K	Ratio of potential evapotranspiration to pan evaporation	0.4-1.5 (–)
	C	The coefficient of deep evapotranspiration	0.01-0.4 (–)
Runoff production	B	The exponent of the tension water capacity curve	0.1-10 (–)
	IMP	The ratio of the impervious to the total area of the basin	0.01-0.15 (–)
Runoff separation	SM	The areal mean of the free water capacity of the surface soil layer	10-80 (mm)
	EX	The exponent of the free water capacity curve	0.6-6 (–)
	CG	The outflow coefficients of the free water storage to groundwater	0.01-0.45 (–)
	CI	The outflow coefficients of the free water storage to interflow	0.01-0.45 (–)
Flow concentration	N	Number of reservoirs in the instantaneous unit hydrograph	0.5-10 (–)
	NK	Common storage coefficient in the instantaneous unit hydrograph	1-20 (–)
	KG	The recession constant of groundwater storage	0.6-1 (–)
	KI	The recession constant of the lower interflow storage	0.9-1 (–)

Table 3 Different cases of synthetic experiments and real catchment case studies for comparison and evaluation

	Data	Hydrological model	Time-varying parameter estimation methods		
			SSC	SSC-DP	Data assimilation
Synthetic experiment	Monthly synthetic data	TMWB model		✓	✓
	Hourly synthetic data	Xinanjiang model	✓	✓	✓
Real catchment case study	Daily data from Wuding River basin	Xinanjiang model	✓	✓	✓
	Daily data from Xun River basin	Xinanjiang model	✓	✓	✓

Table 4 True parameters of different scenarios in the synthetic experiment with the TMWB model

Scenario	Description
1	Both *C* and *SC* are constant
2	Both *C* and *SC* have increasing linear trends and change every month
3	Both *C* and *SC* have periodic variations and change every month
4	Both *C* and *SC* have increasing linear trends and change every six months
5	Both *C* and *SC* have periodic variations and change every six months
6	Both *C* and *SC* have increasing linear trends and change every year
7	Both *C* and *SC* have periodic variations and change every year
8	*C* has a periodic variation with an increasing linear trend, whereas *SC* only has an increasing linear trend. The parameters change every year

Table 5 True parameters of different scenarios in the synthetic experiment with the Xinanjiang model

Scenario	Description
1	*KE*, *CI*, *CG*, *KI*, *KG*, and *NK* remain constant
2	*KE*, *CI*, *CG*, *KI*, *KG*, and *NK* have linear trends and change every month
3	*KE*, *CI*, *CG*, *KI*, *KG*, and *NK* have periodic variations and change every month
4	*KE* has a periodic variation with an increasing linear trend, whereas *CI*, *CG*, *KI*, *KG*, and *NK* only have periodic variations. The parameters change every month

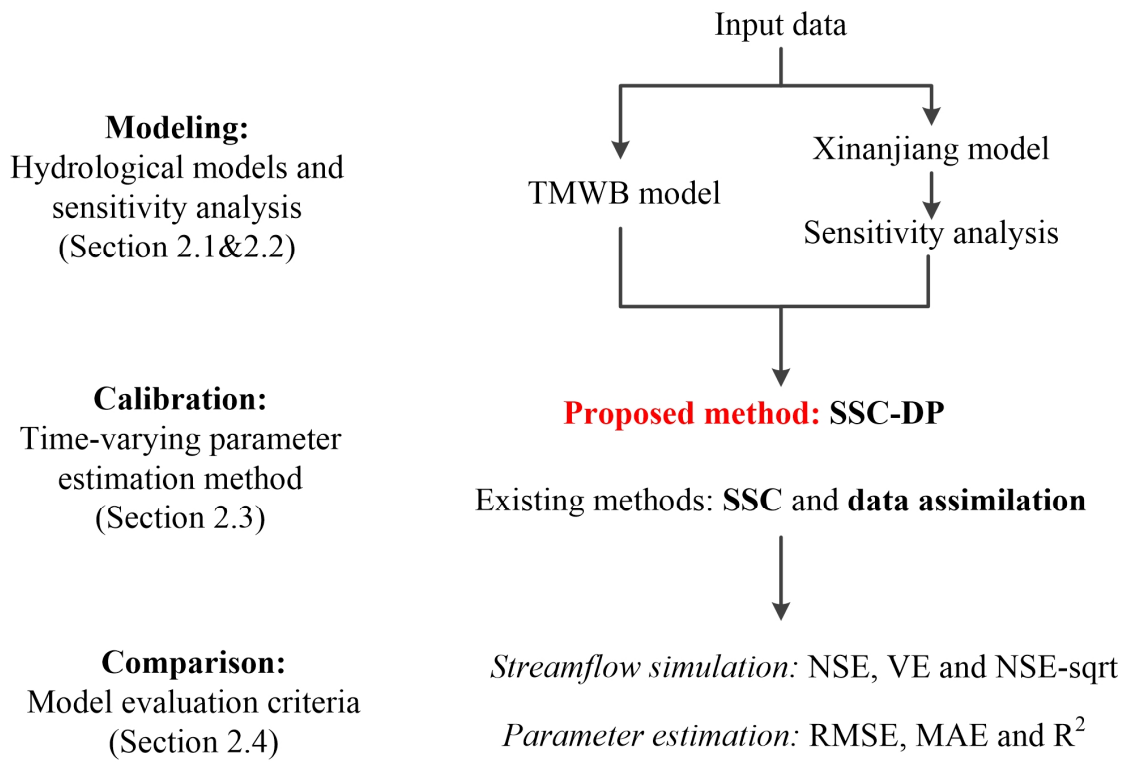

Figure 1 Flowchart of the methodologies

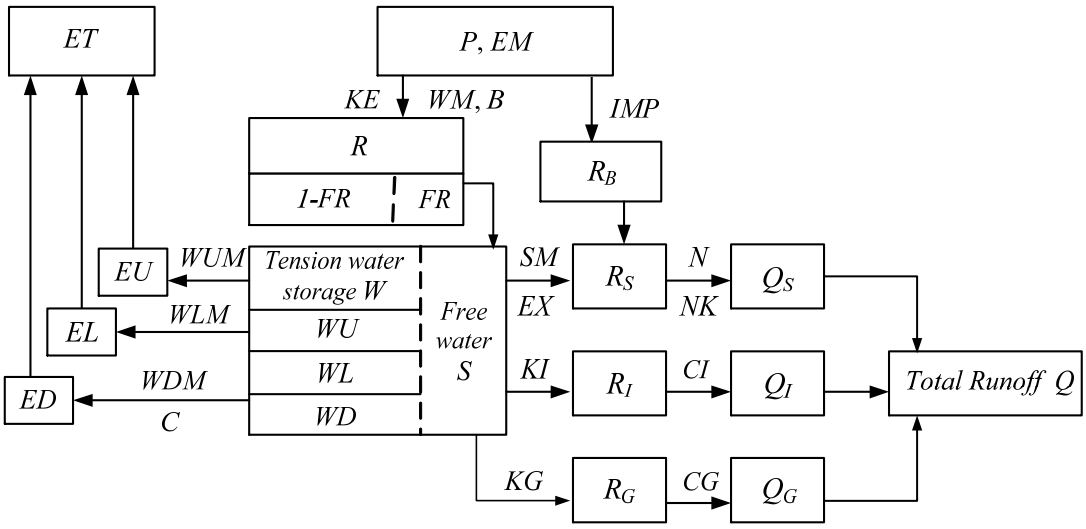

Figure 2 Flowchart of the Xinanjiang model.

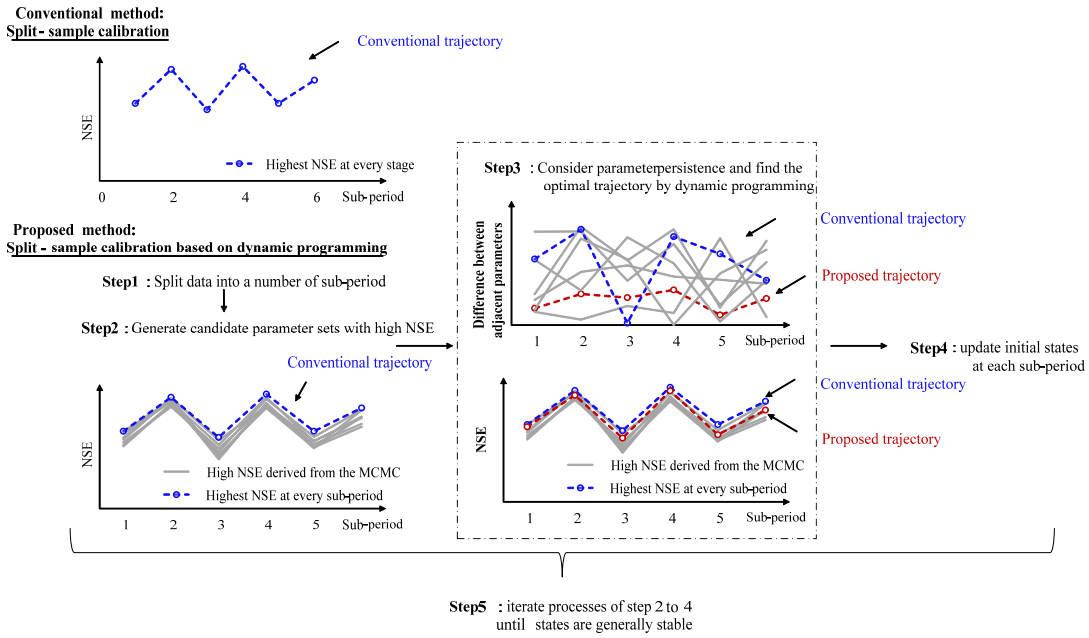

Figure 3 Flowchart of SSC-DP.

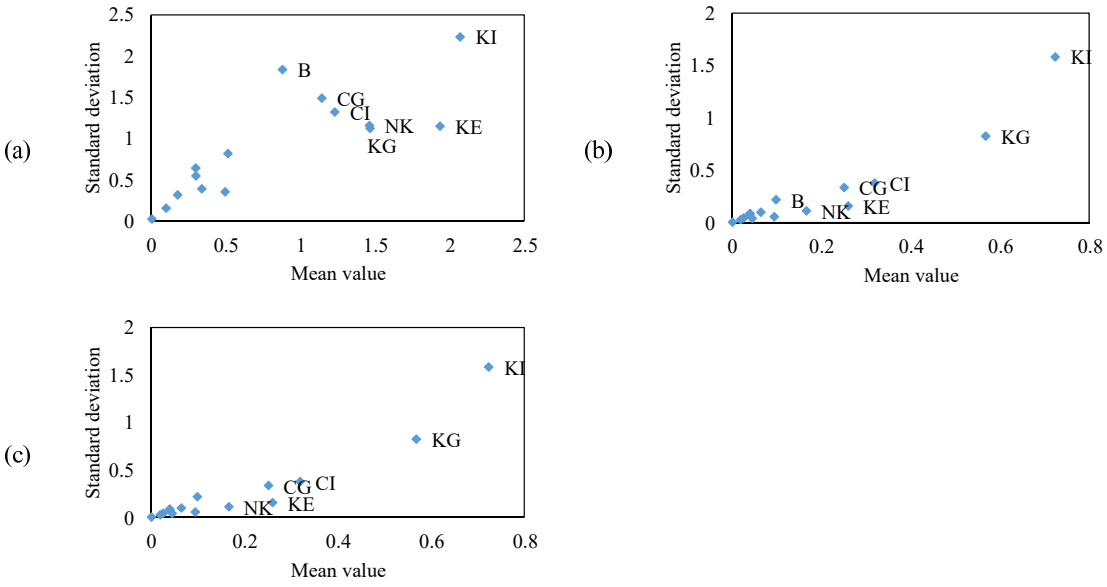

Figure 4 Results of the Morris method for the synthetic experiment with the Xinanjiang model. The sensitivity analysis is based on three different kinds of model responses: (a) NSE; (b) NSE_{abs}; (c) NSE_{ln}. Only the most sensitive parameters are labeled.

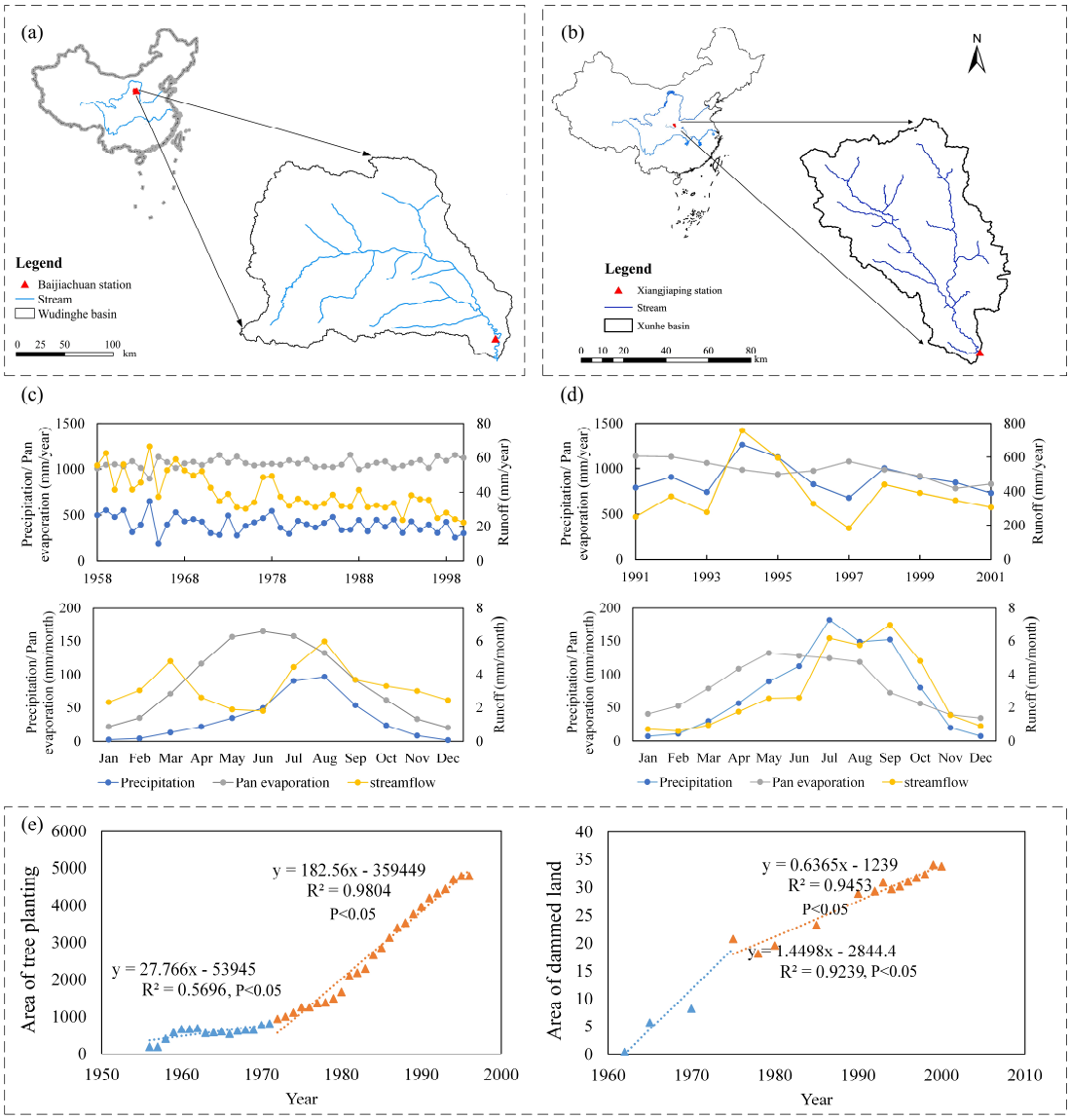

Figure 5 Location of (a) Wuding River basin and (b) Xun River basin. The plots (c) and (d) show the average yearly and monthly variations of precipitation, pan evaporation and streamflow in the Wuding River basin and Xun River basin, respectively. The plot (e) shows the temporal variations in the soil and water conservation measures undertaken in the Wuding River basin.

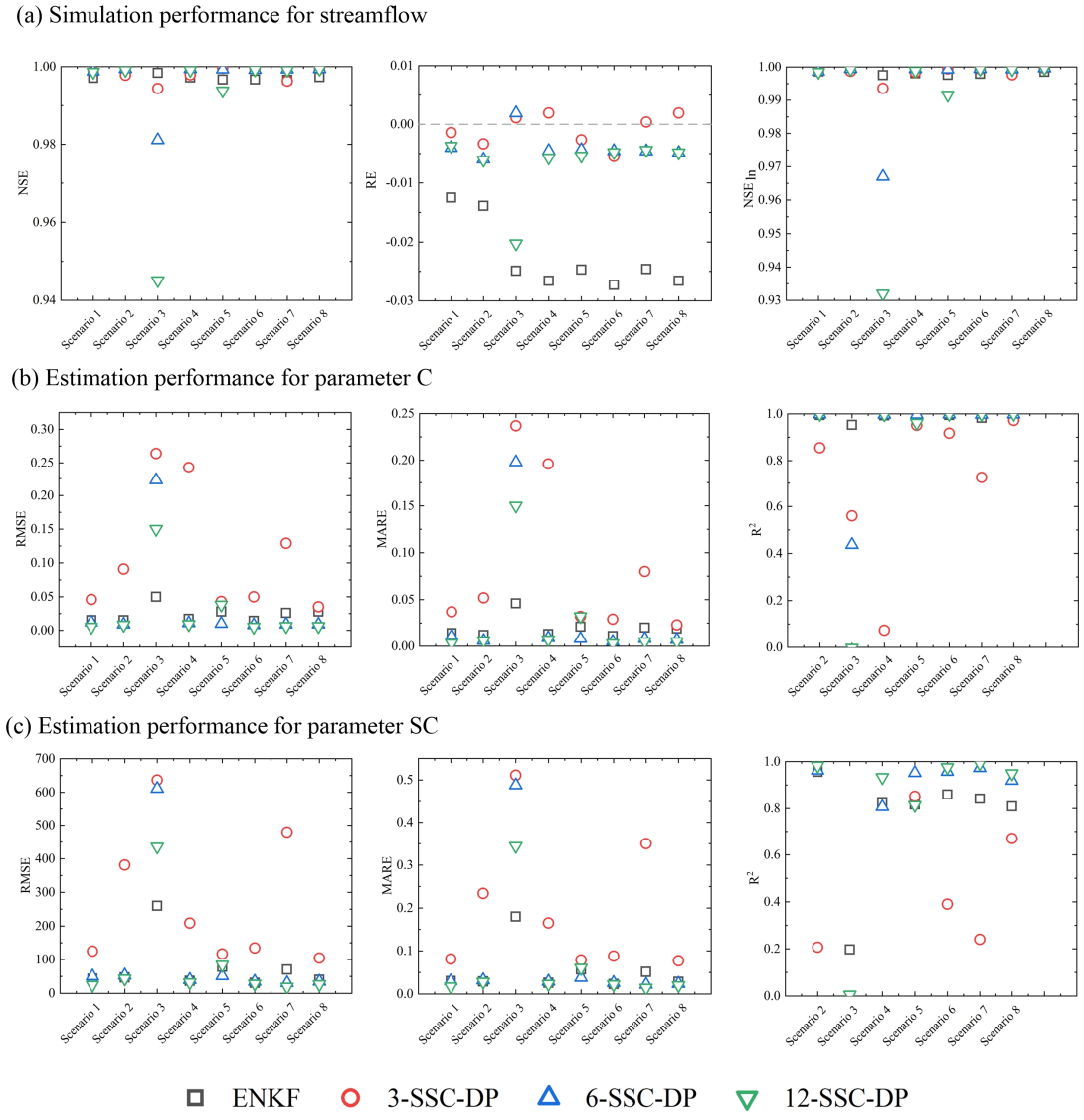

Figure 6 Comparison between the EnKF and SSC-DP methods for (a) streamflow simulation and identification of (b) parameter C and (c) parameter SC.

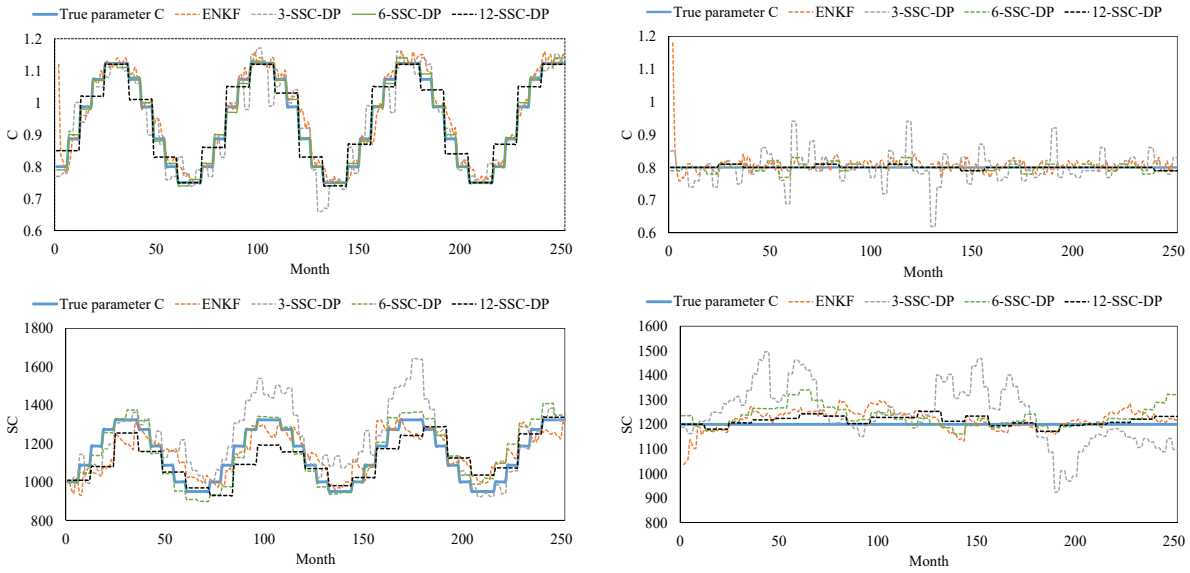

Figure 7 Comparison among different methods for (a) scenario 5 and (b) scenario 1 of the synthetic experiment with the TMWB model.

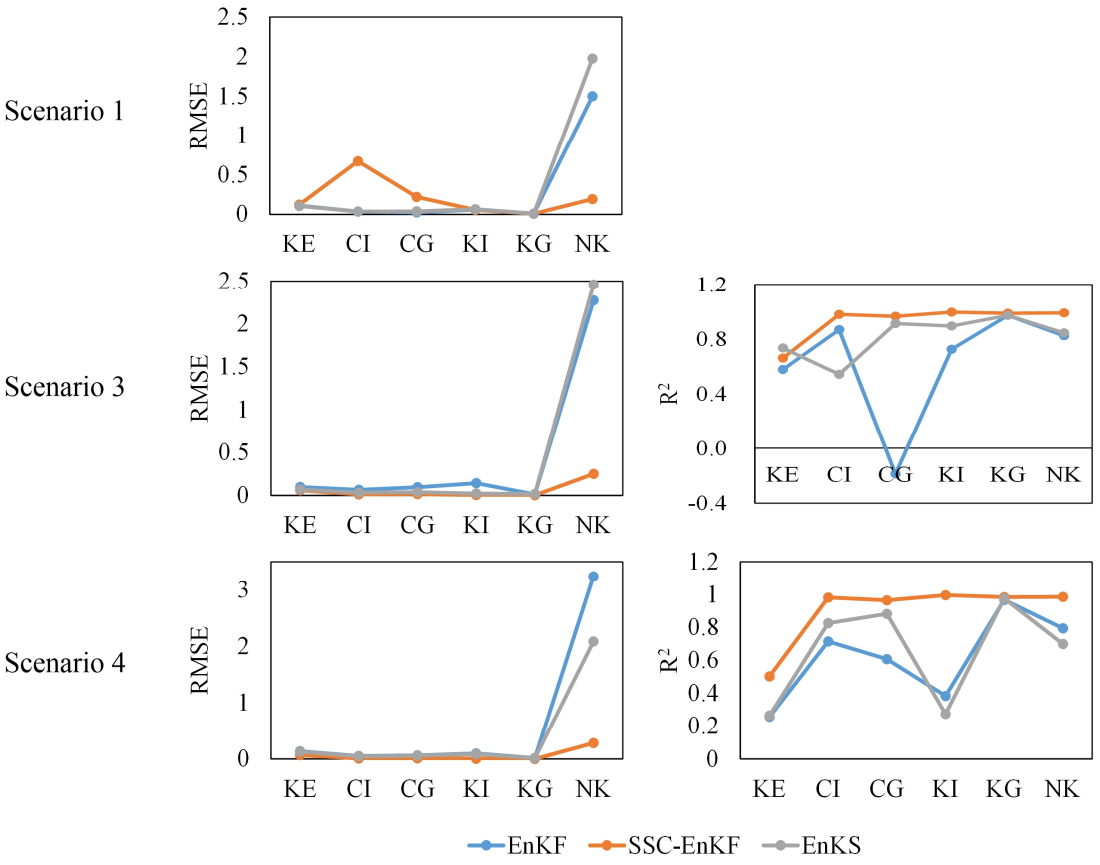

Figure 8 Comparison among EnKF, SSC-EnKF, and EnKS in the synthetic experiment with the Xinanjiang model.

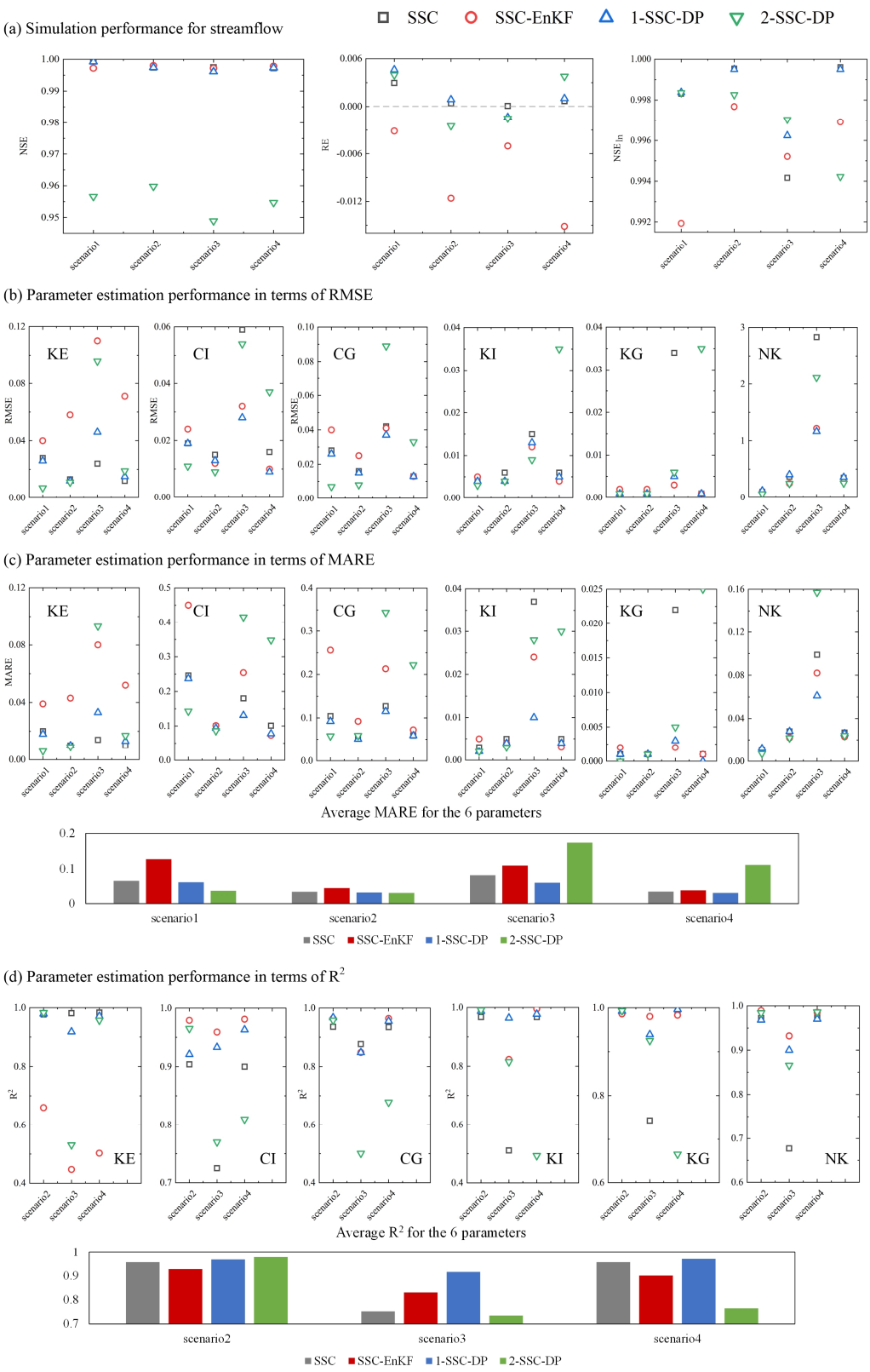

Figure 9 Comparison among the SSC, SSC-EnKF and SSC-DP methods in the synthetic experiment with the Xinanjiang model for (a) streamflow simulation and parameter identification in terms of (b) RMSE, (c) MARE and (d) R^2.

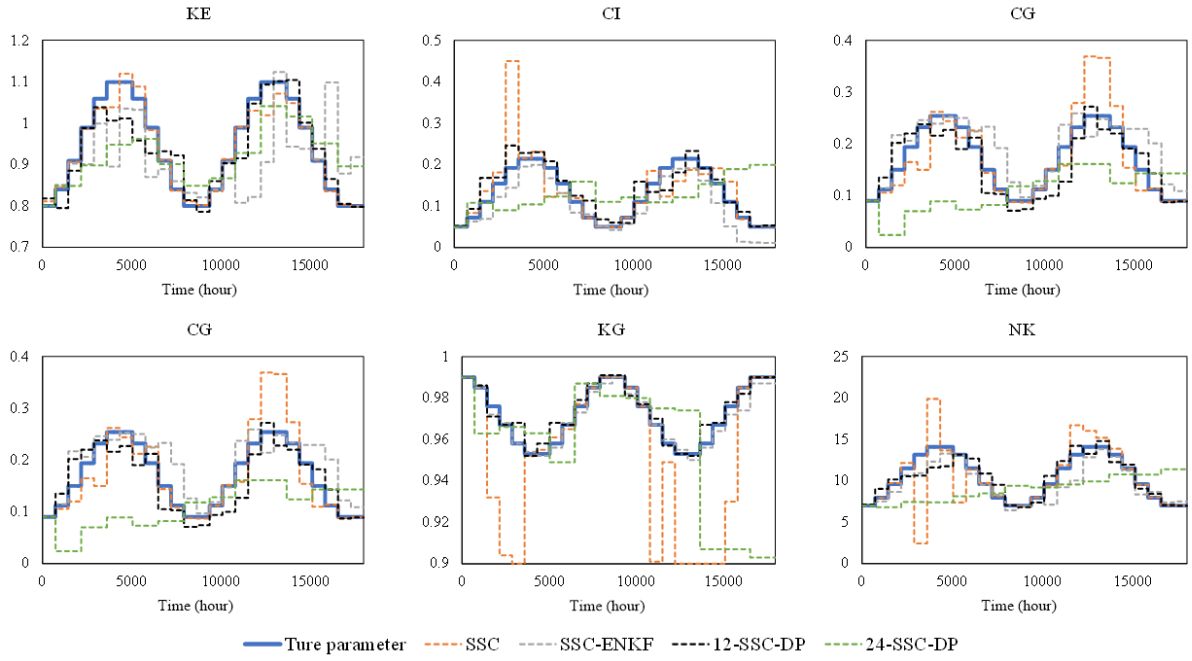

Figure 10 Comparison between estimated parameters and their true values for scenario 3 of the synthetic experiment with the Xinanjiang model.

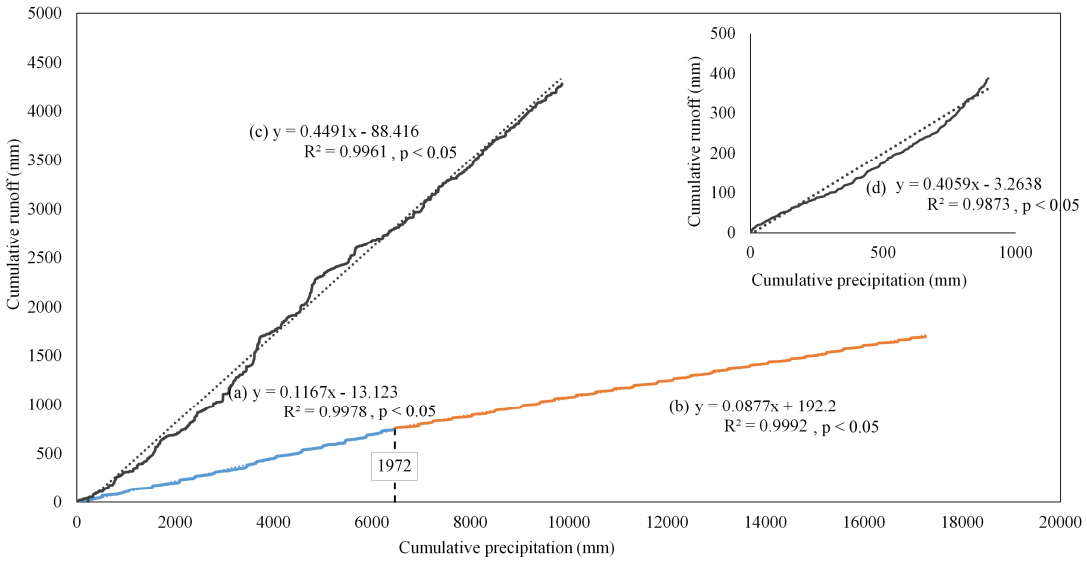

Figure 11 Double mass curves between daily runoff and precipitation for (a) Wuding River basin from 1958–1972; (b) Wuding River basin from 1973–2000; (c) Xun River basin from 1991–2001. Subgraph (d) represents the double mass curve between the mean daily runoff and precipitation from 1991–2001.

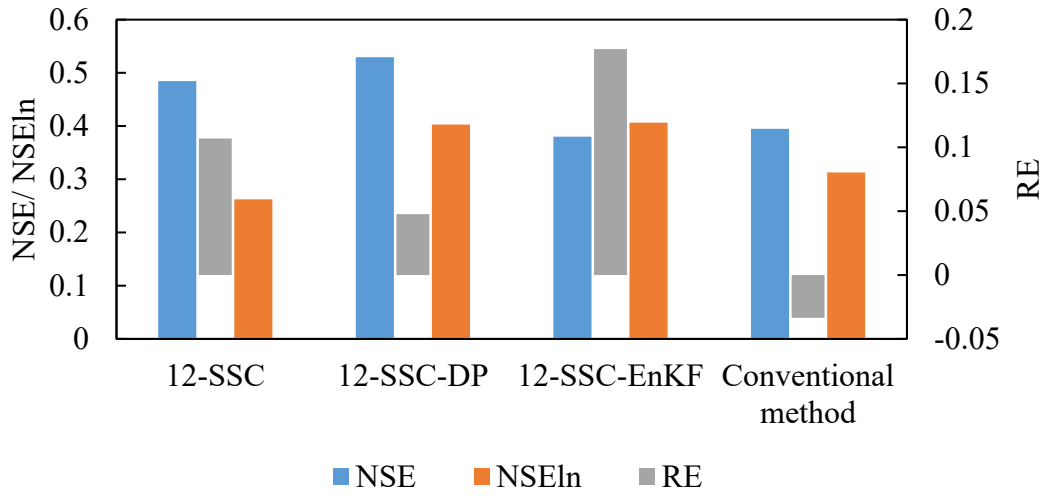

Figure 12 Simulation performance for streamflow in the Wuding River basin. The results of NSE and NSEln are shown on the primary axis, while the values of RE are shown on the secondary axis.

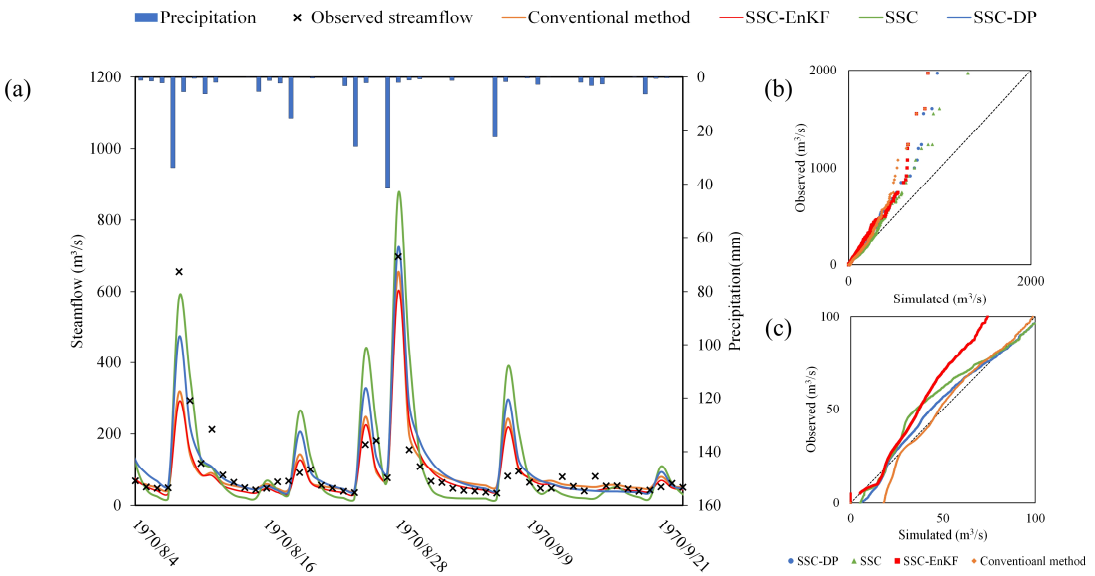

Figure 13 The simulated and observed streamflow using the conventional method, SSC-EnKF, SSC, and SSC-DP for the Wuding River basin. (a) Streamflow simulation hydrograph; (b) The quantile-quantile plot for all streamflow; (c) The quantile-quantile plot for streamflow lower than 100 m^3/s.

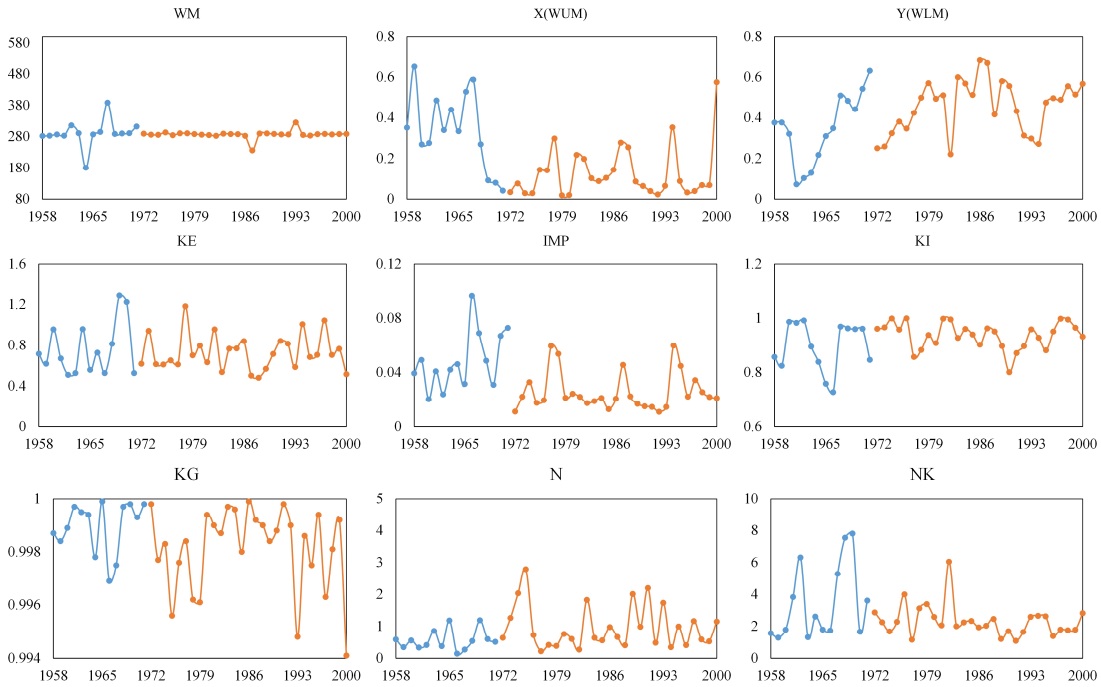

Figure 14 Estimated sensitive parameters of the Xinanjiang model for the Wuding River basin. The blue and orange solid lines represent the estimated parameters pre- and post-1972, respectively.

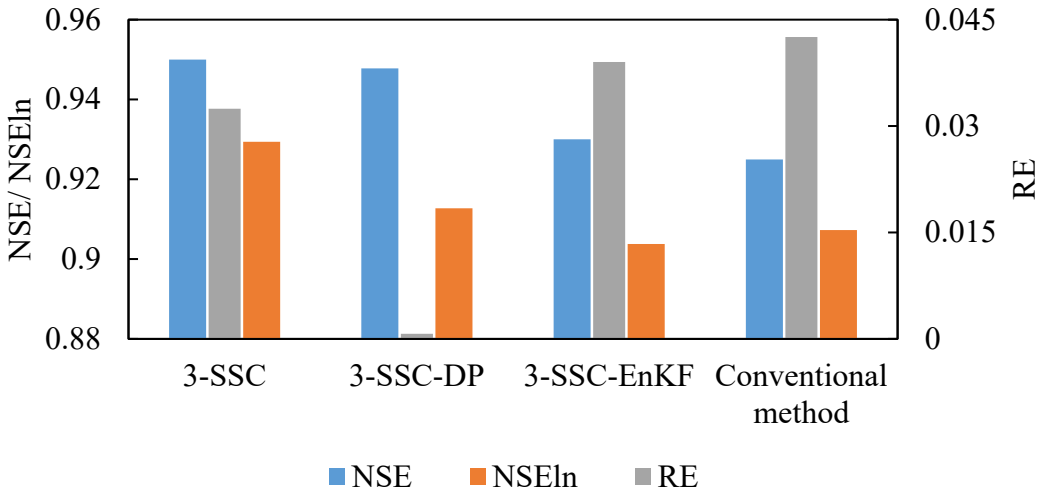

Figure 15 Simulation performance for streamflow in the Xun River basin. The results of NSE and NSEln are shown on the primary axis, while the values of RE are shown on the secondary axis.

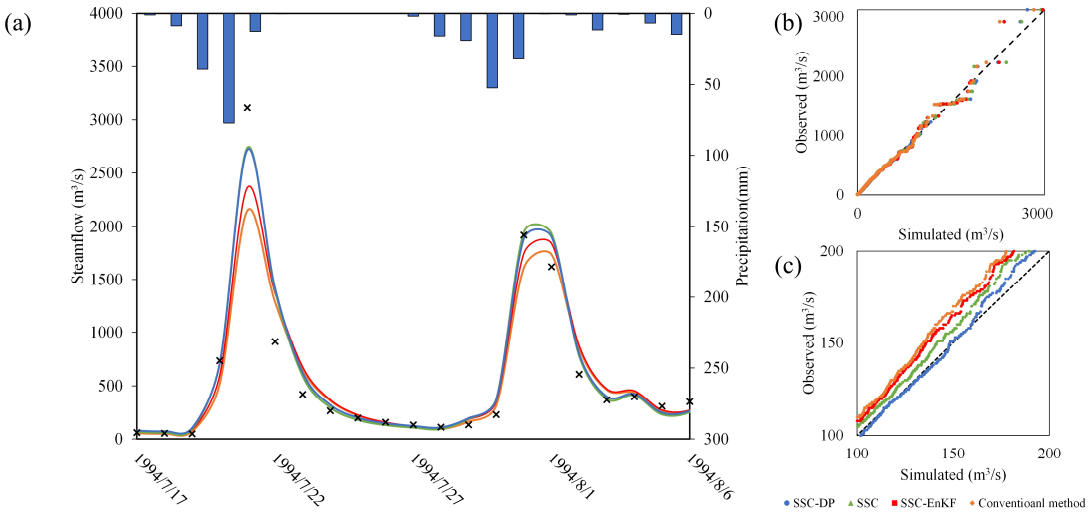

Figure 16 The simulated and observed streamflow using the conventional method, SSC-EnKF, SSC, and SSC-DP for the Xun River basin. (a) Streamflow simulation hydrograph; (b) The quantile-quantile plot for all streamflow; (c) The quantile-quantile plot for streamflow ranging from 100 m^3/s to 200 m^3/s.

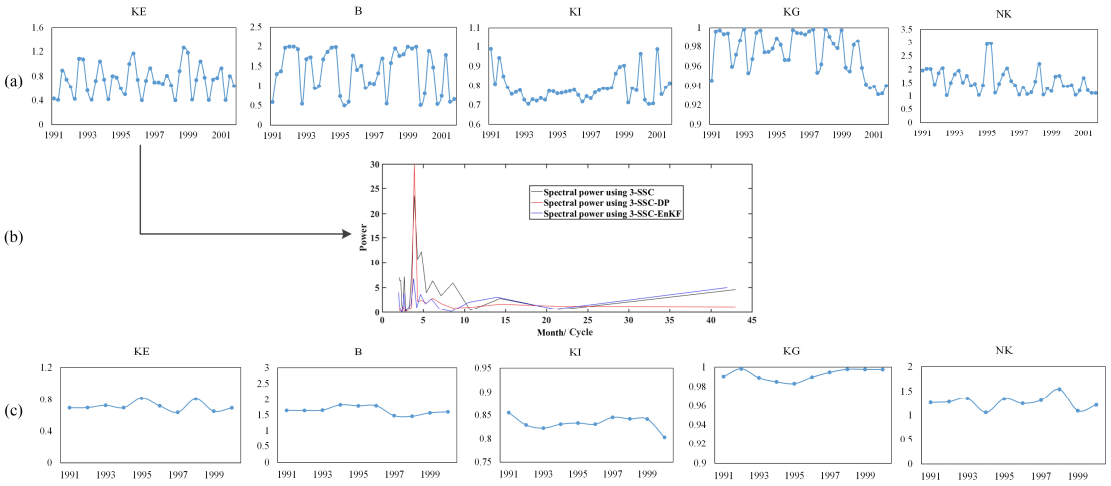

Figure 17 Estimated sensitive parameters of the Xinanjiang model for the Xun River basin over (a) seasonal time scale and (c) annual time scale. Plot (b) illustrates the spectral power of parameter KE using different methods.

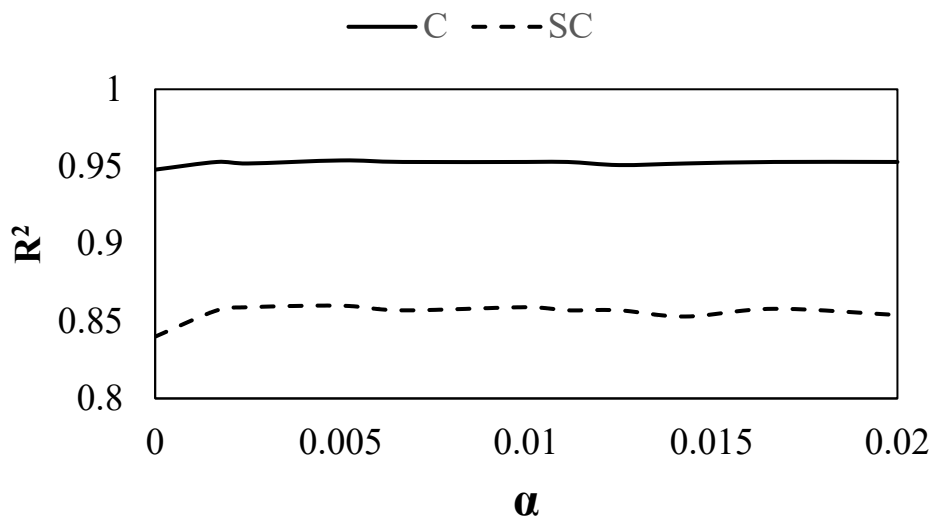

(a)

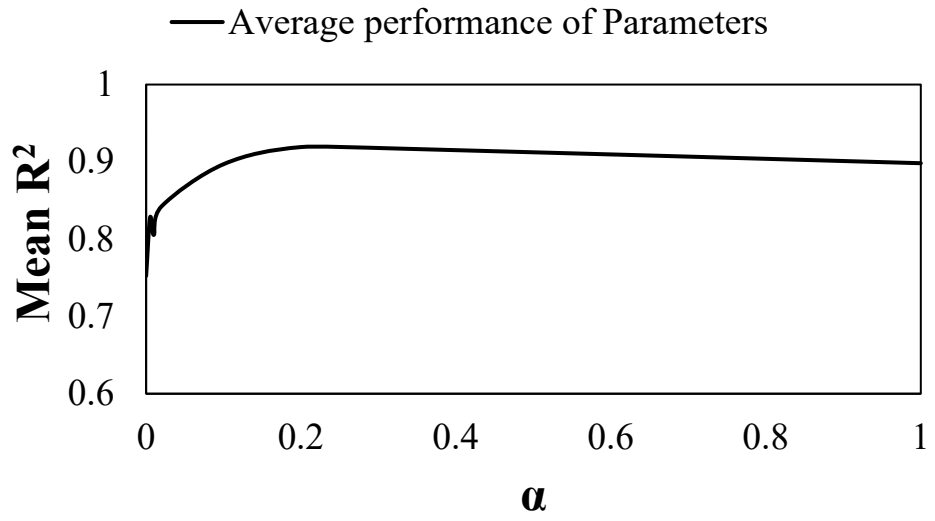

(b)

Figure 18 Correlation efficiency results of SSC-DP using different weights of parameter continuity for synthetic experiments with (a) TMWB model and (b) Xinanjiang model. The mean R^2 is the average value of the R^2 such that the identification results for parameters with different ranges can be summarized.